2013

# Capturing and Modeling a Three-Dimensional Stationary Noise Source Directivity Pattern with a Dynamic Array in the Near Field

Randy Mieskoski
*Wright State University*

# CAPTURING AND MODELING A THREE-DIMENSIONAL STATIONARY NOISE SOURCE DIRECTIVITY PATTERN WITH A DYNAMIC ARRAY IN THE NEAR FIELD

A thesis submitted in partial fulfillment of the

requirements for the degree of

Master of Science

By

RANDY SCOTT MIESKOSKI
B.S., University of Cincinnati, 2000

2013
Wright State University

WRIGHT STATE UNIVERSITY

GRADUATE SCHOOL

October 28, 2013

I HEREBY RECOMMEND THAT THE THESIS PREPARED UNDER MY SUPERVISION BY Randy Scott Mieskoski ENTITLED Capturing and Modeling a Three-Dimensional Stationary Noise Source Directivity Pattern with a Dynamic Array in the Near Field BE ACCEPTED IN PARTIAL FULFILMENT OF THE REQUIREMENTS FOR THE DEGREE OF Master of Science.

_____

Frank Mobley, Ph.D.
Thesis Co-Director

_____

Douglas Petkie, Ph.D.
Chair, Department of Physics
Thesis Co-Director

Committee on
Final Examination

_____
Douglas Petkie, Ph.D.

_____
Ivan Medvedev, Ph.D.

_____
Frank Mobley, Ph.D.

_____
R. William Ayres, Ph.D.
Interim Dean, Graduate School

ABSTRACT

Mieskoski, Randy Scott. M.S. Physics, Department of Physics, Wright State University, 2013. Capturing and Modeling a Three-Dimensional Stationary Noise Source Directivity Pattern with a Dynamic Array in the Near Field.

The author has studied several legacy landmark methodologies to develop an original measurement technique. Spherical harmonics modeling practices were leveraged to accurately represent a source directivity pattern. In this thesis a lightweight microphone measurement array that was manually maneuvered around a static noise source was employed. The measurement technique consisted of inserting a head-tracker sensor onto the microphone array to allow the location of the captured acoustic Sound Pressure Level (SPL) to be investigated. By leveraging the historical methodologies the acoustic SPL and location data collected with this technique were processes to represent a directivity pattern of the compressor source chosen. The results indicated that the measurement technique is valid for capturing acoustic SPL and location data of a static noise source with a dynamic array. Propagation techniques yielded a ten decibel difference between the measured and predicated SPLs. The dynamic measurement technique and method for characterizing the three-dimensional acoustic directivity of a static noise source is further presented in this thesis.

TABLE OF CONTENTS

**I. INTRODUCTION** ..... **1**

**II. BACKGROUND** ..... **8**

DYNAMIC SOURCE – STATIC ARRAY ..... 8

*The Rotorcraft Noise Model* ..... *8*

Measurement array evolution ..... 8

Source noise directivity pattern construction ..... 13

*FLULA2* ..... *14*

Measurement array ..... 14

Source noise directivity pattern construction ..... 15

STATIC SOURCE-STATIC ARRAY ..... 19

*Planar Near Field Acoustic Holography* ..... *19*

Measurement array ..... 21

Source noise directivity pattern construction ..... 23

*Spherical Near Field Acoustic Holography* ..... *24*

Measurement array ..... 25

Source noise directivity pattern construction ..... 26

STATIC SOURCE – MANUALLY MANEUVERED DYNAMIC ARRAY ..... 31

**III. METHODS** ..... **32**

EXPERIMENTAL DESIGN ..... 32

INSTRUMENTATION ..... 36

SOURCE CONSTRUCTION ..... 43

DATA ACQUISITION SOFTWARE DESIGN ..... 45

DATA ACQUISITION ..... 53

*Data Acquisition Technique* ..... *62*

*Analysis* ..... *66*

**IV. DATA** ..... **71**

COEFFICIENT OF DETERMINATION VERSUS FREQUENCY ..... 74

COEFFICIENT OF DETERMINATION VERSUS SPHERICAL HARMONIC ORDER ..... 77

VALIDATION ..... 79

**V. DISCUSSION** ..... **82**

**VI. CONCLUSIONS** ..... **88**

**BIBLIOGRAPHY** ..... **92**

**APPENDIX A** ..... **94**

LIST OF FIGURES

Figure 1. Original 30 Microphone "Goal Post" Array (Conner, Burley, & Smith, 2006) ..... 9

Figure 2. Modified "Goal Post" 30 Microphone Array (Conner, Burley, & Smith, 2006) ..... 10

Figure 3. Vertical Array 800 Feet Apart(Conner, Burley, & Smith, 2006) ..... 11

Figure 4. Array for Ascent and Descent Measurements (Conner, Burley, & Smith, 2006) ..... 12

Figure 5. "Goal Post" Array with 22 Microphones Including WAMS (Conner D. A., 2002) ..... 13

Figure 6. RNM Assembled Hemisphere Representation (Conner, Burley, & Smith, 2006) ..... 14

Figure 7. FLULA2 "Goal Post" or "U-Shaped" Microphone Array (Krebs W. , Butikofer, Pluss, & Thomann, 2003) ..... 16

Figure 8. Coordinate System Reference (Krebs W. , Butikofer, Pluss, & Thomann, 2003) ..... 18

Figure 9. Planar Array Constructed for a NAH Measurement (James, et al., 2011) ..... 22

Figure 10. Measured SPL Map Overlaid on a F-22 Photo at the Approximate Location of Measurement (James, et al., 2011) ..... 24

Figure 11. Dual, concentric 64 Microphone SMA with baffler (Parthy, Jin, & Schaik, 2009) ..... 25

Figure 12. Holographic Projection Example where Coefficients have not been combined (Parthy, Jin, & Schaik, 2009) ..... 29

Figure 13. Combination Projection and Rigid Projection (Parthy, Jin, & Schaik, 2009) ..... 30

Figure 14. Anechoic Chamber Measurement Setup ..... 34

Figure 15. Source and Stationary Validation Microphone ..... 35

Figure 16. G.R.A.S. Microphone and NI9233 USB Four Channel Carrier ..... 37

Figure 17. Head-tracker Components ..... 39

Figure 18. Head-tracker Cube with Axis ..... 40

Figure 19. Array Microphone and Head-tracker Sensor ..... 41

Figure 20. Assembled array with the G.R.A.S. microphone and the head-tracker sensor incorporated with a 5 foot dowel. ..... 42

Figure 21. Air Compressor Model and Information Sticker ..... 46

Figure 22. NI LabVIEW Block Diagram for Head Tracker Data Acquisition Only ..... 48

Figure 23. NI LabVIEW Block Diagram for Acoustic Data Acquisition Only ..... 49

Figure 24. NI LabVIEW Acoustic and Headtracker Data Acquisition Program Block Diagram. ..... 50

Figure 25. LabVIEW Front Panel for Data Acquisition ..... 52

Figure 26. Data Collection Software Functionality Test Set Up ..... 54

Figure 27. Microphone and Head Tracker Set Up for Functionality Test ..... 55

Figure 28. Array Operator Conducting Data Collection ..... 57

Figure 29. Second Data Collection Set Up ..... 60

Figure 30. Second Collection with Validation Microphone ..... 61

Figure 31. Real-time Feedback Visualization Panel ..... 63

Figure 32. Spherical Coordinate System Used in this Thesis ..... 66

Figure 33. Three-dimensional scatter plots of (a) measured and (b) predicted source noise directivity pattern at a normalized distance of one meter and spherical harmonic order of five. 71

Figure 34. Waveform graph depicting the measured (red) and predicted (white) spectrum acquired over the entire measurement and computed for spherical harmonic order five. ..... 72

Figure 35. Plot representing accepted 31 frequencies of the one-third octave band with the corresponding coefficient of determination at spherical harmonic orders one, three, five, seven and ten. ..... 74

Figure 36. Plot representing the accepted frequencies to 300 Hz of the one-third octave band with the corresponding coefficient of determination at spherical harmonic orders one, three, five, seven and ten. ..... 75

Figure 37. Plot representing the accepted frequencies to 1000 Hz of the one-third octave band with the corresponding coefficient of determination at spherical harmonic orders one, three, five, seven and ten plotted on a logarithmic scale. ..... 76

Figure 38. Plot of the coefficient of determination at spherical harmonic orders one, three, five, seven and ten at 125 Hz reference frequency. ..... 77

Figure 39. Plot of the coefficient of determination at spherical harmonic orders one, three, five, seven and ten at the second reference frequency of 6300 Hz. ..... 78

Figure 40. Plot of the mean validation SPL data, the standard deviation of the validation SPL data and the propagated SPL at two meters for each of the selected spherical harmonic orders at the 31 frequencies. ..... 80

Figure 41. Plot of the mean validation SPL data, the standard deviation of the validation SPL data and the propagated SPL at two meters for each of the selected spherical harmonic orders at the 31 frequencies on logarithmic scale. ..... 81

Figure 42. Plot of the mean validation SPL data, the standard deviation of the validation SPL data and the propagated SPL at two meters for spherical harmonic order n=5 at the 31 frequencies. ..... 85

Figure 43. Plot of the mean validation SPL data, the standard deviation of the validation SPL data and the propagated SPL at two meters for spherical harmonic order n=5 reduced to 100 Hz. ..... 86

Figure 44. . Plot of the mean validation SPL data, the standard deviation of the validation SPL data and the propagated SPL at two meters for each of the selected spherical harmonic orders at the 31 frequencies on logarithmic scale. ..... 87

Figure 45. Coefficients of determination for the five orders selected at each of the accepted 31 frequencies. ..... 94

Figure 46. Propagated SPL at two meters for the five orders selected at each of the accepted 31 frequencies ..... 95

**Figure 47. Propagated SPL normalized at one meter for the five orders selected at each of the accepted 31 frequencies.** ..... 96

LIST OF TABLES

Table 1. Examples of Array Positions from F-22 NAH Data Collection (James, et al., 2011) ..... 23

Table 2. Total Relative Error (TRE) Pressure Field Estimates (Parthy, Jin, & Schaik, 2009) ..... 31

## I. INTRODUCTION

Intense sound sources in aeroacoustic applications have historically created an issue with noise exposure to individuals in proximity, and potentially to the community as a whole (Shaw, 1996) (Borsky, 1979) (Galloway, 1974) (Stansfeld S, 2000) (Weinstein, 1982)(National Aeronautics and Space Administration, 1991) (Passchier, 2000). To address and mitigate this noise, the major airframe and engine companies made extensive use of airplane flyover-noise measurements for research and development during the 1960's and 1970's. The prime purposes of these measurements were to define the noise characteristics of the engines and aircraft. It was also to assist in the development of modified engines and/or nacelles that would reduce flyover-noise levels (National Aeronautics and Space Administration, 1991).

By the early 1970s the United States Air Force (USAF) was developing a series of models that were able to simulate aircraft noise in various environments (National Aeronautics and Space Administration, 1991). In 1974 the USAF and Wyle Laboratories conceptually outlined a program that would determine noise exposure due to aeroacoustic emissions (Moulton, 1992). The noise exposure model, or NOISEMAP, was the name given to the FORTRAN program developed to calculate aeroacoustic noise exposure due to aircraft flight, maintenance and ground run-up operations (Moulton, 1992) (Plotkin, 2001). NOISEMAP required that the sound source data was formatted so that it could be stored in the NOISEFILE database. (Moulton, 1992).

NOISEMAP used a dynamic source and static microphone array for creation of a point source representation of the aeroacoustic noise emissions (Moulton, 1992). This method parallels the foundation of electromagnetic theory which begins by examining a point source (Griffiths, 1999) (Eyges, 1972) (Wangsness, 1986) (Jackson, 1999). NOISEMAP extracted aircraft speed, power setting, and noise data from its database, which was created through integrating the sound exposure level (SEL) from a flyover (Plotkin, 2001) (Moulton, 1992).

The data was compiled in card form for use on a mainframe computer and NOISEMAP itself was designed to operate on an 80386 or 80286 microprocessor with at least one megabyte of memory (Moulton, 1992) (Page, Plotkin, & Wilmer, 2008) (Plotkin, 2001). While novel for its time, NOISEMAP was restricted by the technology; it could not support or sustain complex geometries, therefore it was not able to accurately represent an acoustic noise source (Plotkin, 2001).

Due to measurements accomplished at Narvik Norway, the Air Force Research Laboratory (AFRL) and Wyle Laboratories were able to show the limitations of this integrated noise model method (Plotkin, 2001). By the 1990s AFRL was able to move NOISEMAP from a mainframe computer into a PC application. This advance in computing technology allowed for more processing power to address the limitations of NOISEMAP and made simulation practical for a larger range of acoustical problems than in the past. With the availability of the National Geospatial Intelligence Agency (NGA) Digital Elevation Model (DEM) and the US Geological Survey (USGS) Digital Terrain Elevation Data (DTED), Wyle Laboratories, in conjunction with the

National Parks Service (NPS), proposed incorporating topographical effects into NOISEMAP (Plotkin, 2001). The simulation model NoiseMap SIMulation (NMSIM) was used for examining the effect of wind and temperature gradients on noise signatures. NMSIM expanded the NOISEMAP point source model by utilizing numeric curve fits and adding in polar directivity and magnitude. This was again completed in similar fashion to electromagnetic theory development in multi-pole expansion. Now a better sound source representation was available than what was utilized in NOISEMAP(Moulton, 1992) (Plotkin, 2001) (Page, Plotkin, & Wilmer, 2008) (Jackson, 1999) (Griffiths, 1999) (Wangsness, 1986) (Eyges, 1972).

The original purpose of NMSIM was to validate proposed propagation algorithms for use in NOISEMAP (Plotkin, 2001). However, NMSIM proved itself useful for the detailed demonstration of the noise associated with individual events and in terrain analysis (Plotkin, 2001) (Moulton, 1992). For instance, around a national site, such as the Grand Canyon, there are popular tourist activities that allow the site to be viewed from the air. This is accomplished by use of a variety of air tour aircraft that produce noise. The NPS realized the potential for noise pollution and applied NMSIM to an analysis of aircraft noise in the Grand Canyon. The NPS had “a goal of half of the park being noise-free three quarters of the time” (Plotkin, 2001). NMSIM aided the NPS in protecting the integrity of the soundscape through the use of modeling noise with terrain analysis (Plotkin, 2001).

While NMSIM offered substantial advantages to its predecessor NOISEMAP like the inclusion of terrain and a polar directional source, it was still limited. While the two-dimensional

source representation was better than the point source, it did not contain any elevation directivity. NIMSIM also required increasingly more computer power to produce noise contours (Page, Plotkin, & Hobbs, Acoustic Repropagation Technique version 3 (ART3), 2004) (Krebs & Thomann, 2008) (Moulton, 1992) (Page & Plotkin, Acoustic Repropagation Technique Version 2 (ART2), 2001).

Advances in computing power would assist in further developing the NMSIM noise contour efforts. However, in order to address the elevation directivity, noise emissions from rotary-wing aircraft were examined to develop a more accurate source modeling technique. As the use of rotary-wing aircraft in civilian aeronautics became more typical there was no model available to adequately represent noise emission from this type of aircraft. The increased use of rotary-wing aircraft created a natural and logical step to explore rotorcraft as an aeroacoustic noise source (Page, Plotkin, & Wilmer, 2008). Due to the three-dimensional nature of the rotary-wing directivity pattern, both NOISEMAP and NMSIM failed to capture and model rotorcraft noise (Page, Plotkin, & Wilmer, 2008) (Krebs, Butikofer, Pluss, & Thomann, 2003) (Ollerhead, 1969) (Page & Plotkin, 2001) (Page, Plotkin, & Hobbs, 2004) (Hobbs, Page, & Schultz, 2010). The National Aeronautics and Space Administration (NASA) and Wyle Laboratories accomplished the representation of the three-dimensional nature of rotary-wing acoustics through the Rotorcraft Noise Model (RNM) (Brenter K. S., 1994) (Conner, 2002) (Page, Plotkin, & Wilmer, 2008).

RNM is a computer simulation program, similar to NMSIM, which is used to model sound propagation through the atmosphere. It utilizes a source created through the capture of

a dynamic source of rotorcraft noise with a static linear microphone array, as in NOISEMAP. However, it makes predications by integrating the data that is collected at the microphones and interpolating it to either level ground or mountainous terrain applications (Brenter K. S., 1994) (Conner, 2002) (Smith, 2006).

RNM overcomes some of the limitations of NMSIM by exploiting a database of source noise hemispheres that define the three-dimensional source characteristics over a range of flight conditions (Page, Plotkin, & Wilmer, 2008) (Conner, 2002) (Conner, Burley, & Smith, 2006) (National Aeronautics and Space Administration, 1991). It is noted that numerous factors must be considered to collect accurate data for the database. For instance, vehicle orientation and operating state along with meteorological data at different altitudes and positions relative to the static array are crucial inputs to the construction of the hemispheres (Conner, Burley, & Smith, 2006).

At the same time that RNM was being developed, the Swiss Federal Laboratories began exploring a technique of predicting the A-weighted time history of flyover noise by making use of aeroacoustic directivity patterns. The directivity patterns of the source were based on simultaneous recordings of the acoustical and geometric aircraft data (Pietrzko & Hofmann, 1988). By the late 1990s this new method of deriving a three-dimensional directivity pattern of a noise source based on an expansion of the measurement data with spherical harmonics also incorporated elevation directivity with the polar directivity. Both RNM and the Swiss efforts contributed to developing a three-dimensional representation of a dynamic noise source. It is of

interest to the author to point out that the parallel path of electromagnetic theory development is again referenced by bringing acoustical modeling into full three-dimensional analysis and the use of spherical harmonics (Krebs W. , Butikofer, Pluss, & Thomann, 2003) (Jackson, 1999) (Griffiths, 1999).

Through the turn of the century progress was made to improve the description of the three-dimensional directivity pattern of a sound source and a new model was developed at Swiss Federal Laboratories for Materials Testing and Research (EMPA) called FLULA2 (Krebs, Butikofer, Pluss, & Thomann, 2003) (Krebs & Thomann, 2008). This model defines the source noise level at a reference distance on a sphere. FLULA2 also exploits the mathematical physics application of spherical harmonics (Krebs & Thomann, 2008) (Arfken & Webber, 2001). Originally the FLULA2 model was used to measure fixed wing aircraft. Because of the substantial difference in fixed-wing and rotary-wing aircraft, it was expected that the existing source noise model in FLULA2 was insufficient to describe rotorcraft aeroacoustic noise emissions correctly (Krebs, Butikofer, Pluss, & Thomann, 2003). Initially FLULA2's limiting factor was the inability to model helicopter noise because there are no FLULA2 compatible source data sets for simulating helicopter noise. Specifically the "rotational symmetry was expected to prove unsuitable in describing the directionality of the sound emission" (Krebs & Thomann, 2008). However, by analyzing the measured sound levels with different methods, the model allowed for a full three-dimensional description of the directivity. FLULA2 made use of spherical harmonics and a closed form solution in comparison to RNM replicating rotorcraft data on the surface of a sphere by interpolation pattern (Krebs & Thomann, 2008) (Krebs W. , Butikofer, Pluss, & Thomann, 2003).

The above development of aeroacoustic models, from NOISEMAP to RNM and FLULA2, eventually lead to the three-dimensional representation of the source directivity pattern. Near the turn of the century another measurement and modeling technique was pioneered that also represented the three-dimensional patterns of source noise. This technique is called Near-field Acoustic Holography (NAH). This is a measuring process that can be employed for locating and characterizing stationary sound sources from measurements made by a stationary microphone array (Paillasseur, Thomas, & Pascal, 2011). "NAH has been shown to be a powerful tool for the study of sound radiating from a vibrating source" (Giuseppe, Martarelli, Revel, & Tomasini, 2002). The holography portion of this method enables the experimenter the ability to recognize the acoustic field source to predict the acoustic emission pattern (Lee, 1996).

This thesis intends to leverage the acoustic collection techniques explored above on a static source with a dynamic microphone array. The three-dimensional directivity pattern modeling techniques of RNM and FLULA2 for the modeling of a dynamic acoustic source will serve as an aid in developing a model in the static source case. An apparatus will be constructed for use as a dynamic man portable microphone array which will measure a static acoustic source. The noise source data will then be processed in a similar way as the FLULA2 spherical harmonic techniques in order to model the static acoustic source on a sphere or hemisphere. The static noise source propagation will be collected at a second static microphone in order to validate the dynamic array measurement technique.

## II. BACKGROUND

### Dynamic Source – Static Array

In the preceding section an overview was given in order to identify the historical development of acoustic measurement techniques for specific applications. The following section will explore some of these methods in more detail, for example, cases where the array remained static and the source was dynamic will be investigated. To begin the examination of this case, the three-dimensional Rotorcraft Noise Model will be examined.

#### The Rotorcraft Noise Model

##### *Measurement array evolution*

The results of the NOISEMAP and NMSIM modeling techniques failed to yield a three-dimensional representation of the source noise. In order for NMSIM to contain three-dimensional sources it would have had to include Euler angles in the sound level at a reference distance from the source (Plotkin, 2001).

In the United States, RNM forged the path for three-dimensional modeling of a dynamic source with a static measurement array. The RNM method, known as the Acoustic Repropagation Technique (ART), is based on the capture of a dynamic source of rotorcraft noise with a static linear array. Source noise hemispheres are created from the flyover data captured in acoustic flight test measurements. During a sponsored Acoustic Week flight test in 2003 researchers used NASA Langley's Digital Acoustic Measurement System (DAMS) which consisted of a 30 microphone array. The array was constructed by using three acoustic data vans each

consisting of a 10-microphone system. The microphones were half inch pressure response condenser types with grid caps along with a 4 inch wind screen on each of them. The signals collected by the microphones were low-pass filtered at 11,670 Hz and digitized at the microphone power supply box. The signal was then transmitted by cable to a data van and recorded (Conner, Burley, & Smith, 2006). The ART array was originally intended to be a "goal post" design with 30 microphones as shown in Fig. 1 below.

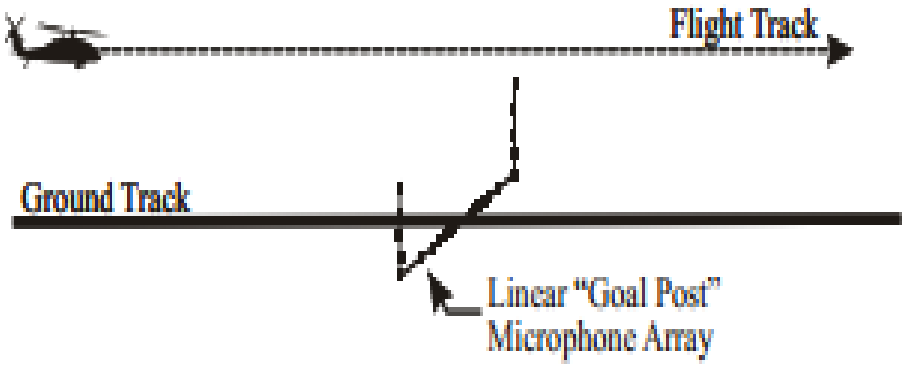


**Figure 1. Original 30 Microphone "Goal Post" Array (Conner, Burley, & Smith, 2006)**

However, for the test purposes, there was an emphasis on acoustic detection signatures. Thus an adjustment to the 30 microphone "goal post" array was made to provide accuracy for the noise measurement forward of the rotorcraft, where the initial acoustic detection typically occurs, thus the justification for the change to the array configuration (Conner, Burley, & Smith, 2006). Vehicle position and orientation to the microphone array were of the utmost importance to develop the hemisphere. For example, the rotor orientation along the flight track relative to the ground microphone array affects projection of the measured acoustic data to the noise hemisphere (Conner, Burley, & Smith, 2006) (Page, Plotkin, & Wilmer, 2008). The array set up was modified to contain two separate arrays as in Fig. 2. This is of importance when evaluating a dynamic array as will be addressed in future sections.

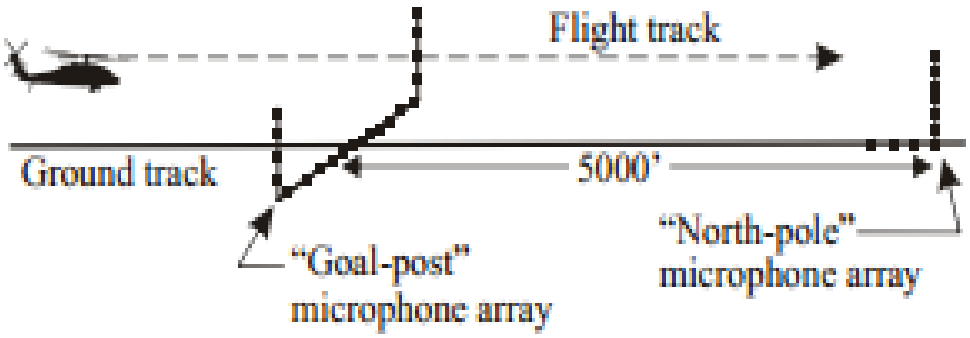


**Figure 2. Modified "Goal Post" 30 Microphone Array (Conner, Burley, & Smith, 2006)**

The "goal post" array was now reduced to 20 microphones and the remaining 8 microphones created a second "north pole" array. The modified "goal post" array now consisted of 12 microphones on the ground. The remaining eight were suspended from two cranes on either side of the flight path, with each crane containing four microphones. There

was a distance of 800 feet between the vertical array portions and the largest height of the microphones was 175 feet as in Fig. 3 (Conner, Burley, & Smith, 2006) (Krebs W. , Butikofer, Pluss, & Thomann, 2003).

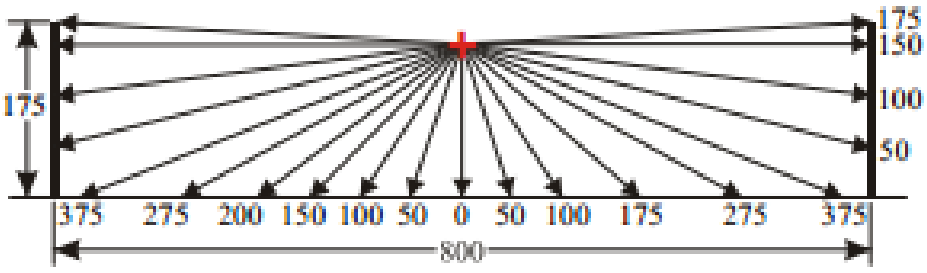


**Figure 3. Vertical Array 800 Feet Apart (Conner, Burley, & Smith, 2006)**

The "north pole" array, Fig. 2, was added to the modified system to gather data that would improve the fidelity of the noise measurement directly in front of the rotorcraft. This array consisted of the remaining 10 microphones. A third crane was used to suspend six of the remaining microphones for the vertical portion of the "north pole" array. These microphones were suspended at heights of 30, 60, 90, 120, 150 and 175 feet above ground level. Four microphones were deployed on the ground at distances of 0, 500, 1000, and 2000 feet from the base of the crane measured towards the "goal post" array as referenced in Fig. 1. (Conner, Burley, & Smith, 2006).

In 2005 another array was designed and deployed in support of RNM and the NASA Heavy Lift Rotorcraft Acoustic Flight Test. This array consisted of the 20 microphone "goal post" array used in the 2003 test with an addition. Two microphones were added on the ground on

each side of the vertical portions of the array at a distance of 1200 feet from the center of the array. This now 22 microphone array was designed to measure source noise hemispheres for level, ascending and descending flight conditions (See Fig 4). During ascent and decent the rotorcraft would be at altitudes in excess of the 150 feet level flight path. The addition of the two side microphones in this array configuration were meant to improve the angular coverage in other than level flight conditions (Conner, Burley, & Smith, 2006).

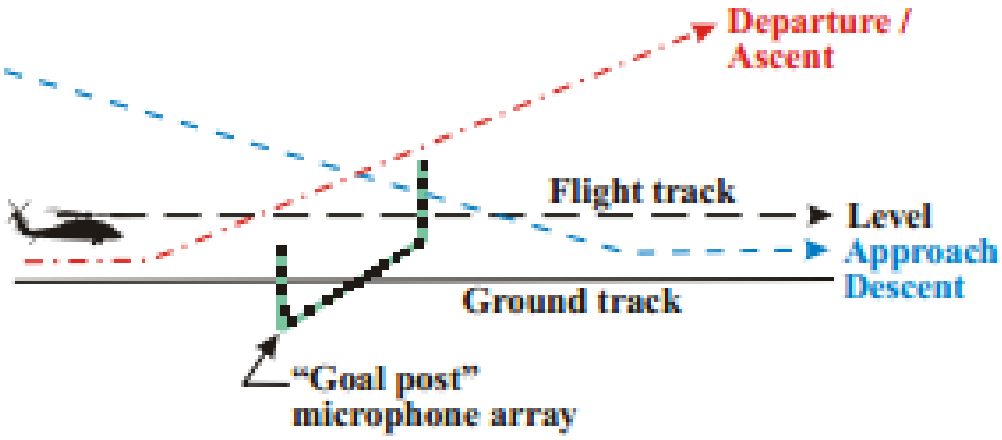


**Figure 4. Array for Ascent and Descent Measurements (Conner, Burley, & Smith, 2006)**

The "goal post" portion of this array construction was using the DAMS set up as in the 2003 test. The two new microphones that were added at the 1200 foot positions along the ground were the Wireless Acoustic Measurement System (WAMS) developed by NASA Langley Research Center (LaRC) as referenced in Fig. 5. WAMS consisted of half-inch pressure response microphones fitted with grid caps and four inch wind screens. WAMS digitized at a 25 kHz sample rate with low-pass filters at 12.5 kHz. The data is recorded on a flash card. The advantages of the WAMS is a greater signal to noise ratio (SNR) resulting in a reduced noise

floor when compared to DAMS. The wireless portion yielded the ability to link microphone and computer remotely from distances as far as 50 miles (Conner, Burley, & Smith, 2006). Rotorcraft then passed through the array at 150 feet altitude.

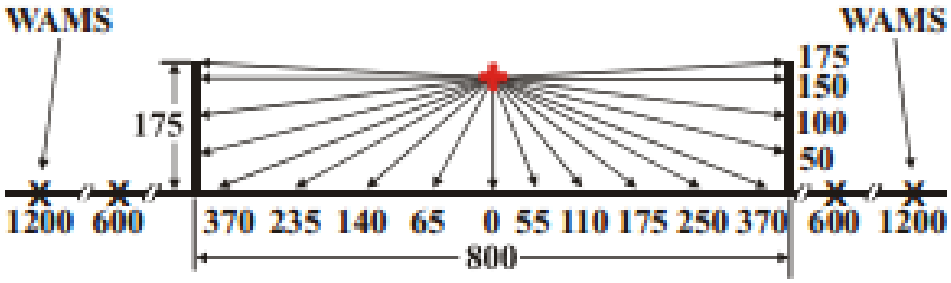


**Figure 5. "Goal Post" Array with 22 Microphones Including WAMS (Conner D. A., 2002)**

### *Source noise directivity pattern construction*

The data collected at the 2003 and 2005 test were then used to build a source noise hemisphere using RNM and the Acoustic Repropagation Technique (ART). The ART program takes into account the effects of spherical spreading, atmospheric absorbsion and ground reflections that were calculated in RNM and integrates the collected microphone data to assemble the hemisphere. The hemisphere is assembled by tracing the measured noise levels back to the source location and then onto a hemisphere of selected constant radius. This fills all of the hemisphere grid points using the measured data resulting in a detailed, high resolution ground noise contour that moves with the vehicle (Conner, Burley, & Smith, 2006). The sound hemispheres can be created either analytically or experimentally from multiple sources with both broadband and pure tone phase as both are acceptable into RNM (Conner D. A., 2002).

Points on the hemisphere are then portrayed with fixed radius and the two traditional spherical angles theta (Θ) and phi ($\varphi$), which represent the standard azimuthal and elevation angles in spherical coordinates. RNM performs the acoustic atmospheric propagation for a given vehicle and creates ground noise predications, detailed time history predictions and other research focused output data (Conner D. A., 2002).

**Figure 6. RNM Assembled Hemisphere Representation (Conner, Burley, & Smith, 2006)**

## FLULA2

In parallel development, scientists at the Swiss Federal Laboratories created a simulation model with limited source directivity descriptions similar to NMSIM. FLULA2 exploited the properties of spherical harmonics which enabled the ability to model dynamic sources measured from static arrays in three-dimensions.

### *Measurement array*

In the fall of 1998 researchers at the Swiss Federal Laboratories for Materials Testing and Research, the acronym used for the Swiss Federal Laboratories is from the German eine Forschungsinstitution im ETH-Bereich (EMPA), conducted numerous measurements or flight passes of dynamic sources using a static "goal post" or U-shaped microphone array. The array was constructed using 13 half inch class one microphones. The array had a width of

approximately 493 feet between vertical portions of the array and a height of roughly 164 feet (See Fig. 7). EMPA was able to capture dynamic rotorcraft flight data with a single array. In comparison RNM utilized two arrays and 30 microphones at a height of 175 feet with the vertical array portion separated by 800 feet. The FLULA2 construct allowed for the noise to be measured simultaneously at all microphone locations as the rotorcraft executed its flight path through the array. The height on each pass was also kept constant at the array height of 164 feet unless flyovers were performed which changed the height as well as the speeds. All 13 microphones were calibrated with an acoustic calibrator prior to each measurement set. Three different helicopters were used in the measurement and their positions were tracked by precision radar and the source orientation was measured by a gyroscope (Krebs W., Butikofer, Pluss, & Thomann, 2003)

### *Source noise directivity pattern construction*

The data was then converted into 24 one-third octave bands using a Norsonic N840 spectrum analysier ranging from 25 Hz to 5000 Hz (Krebs, Butikofer, Pluss, & Thomann, 2003). The measurement data was then used to construct a representation of the source by applying the theory of spherical harmonics (Krebs W. , Butikofer, Pluss, & Thomann, 2003). The measured data at a fixed radius from the center of mass of the aircraft required the use of a normalization equation (Pietrzko & Hofmann, 1988) (See Eqn. 1).

$$SPL_{iR} = SPL_{id} + \alpha_i d - \alpha_{i0} R + 20 log_{10}\left({}^{d}/_{R}\right) + \Delta_i \qquad (1)$$

1) *R* is the radius at a specified directivity pattern

2) SPL is the Sound Pressure Level of the spherical spreading of the waves. This is at the respective one-third octave band
3) $d$ is the propagation from the source to the receiver
4) $\alpha_i$ and $\alpha_o$ are the atmospheric absorption factors in dB $\mathrm{m}^{-1}$
5) $\Delta_i$ is the ground reflection interaction

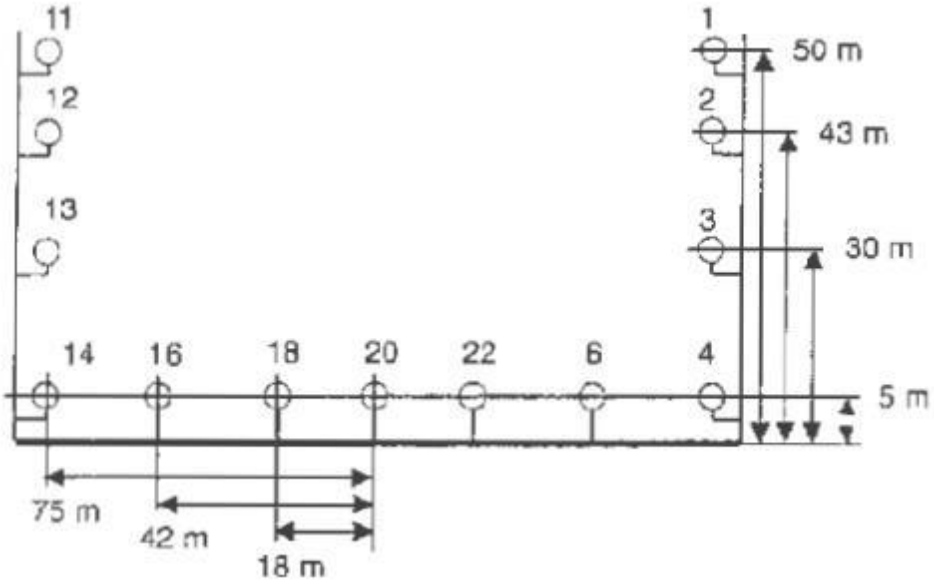


**Figure 7. FLULA2 "Goal Post" or "U-Shaped" Microphone Array (Krebs W. , Butikofer, Pluss, & Thomann, 2003)**

Due to the completeness property of the spherical harmonics, any function $f(\theta, \varphi)$ evaluated on a spherical surface is expanded into a double series of spherical harmonics as referenced in Eqn. 2-3 (Jackson, 1999) (Arfken & Webber, 2001).

$$f(\theta,\varphi) = \sum_{l=0}^{\infty} \sum_{m=-l}^{l} A_{lm}\, Y_{lm}(\theta,\varphi) \quad , \tag{2}$$

where the unknown coefiicients, $A_{lm}$, are then defined as

$$A_{lm} = \int d\Omega\, Y_{lm}^{*}(\theta,\varphi) f(\theta,\varphi) \quad . \tag{3}$$

The method employed uses a least-square analysis to determine the coefficients of a spherical harmonic expansion (Krebs W. , Butikofer, Pluss, & Thomann, 2003). The acoustic data obtained determines the order of the spherical harmonics. Experimental results at EMPA suggest that acceptable results will be obtained with a maximum order of seven.

By applying this method the three-dimensional source emission can be described in terms of one-third octave bands at the normalization distance (Krebs, Butikofer, Pluss, & Thomann, 2003). Mirroring techniques become relevant when data exists for only one side of an aircraft. Similarly, data has to be mirrored into the upper hemisphere prior to the fit where no data exists (Butikofer, 2006). After the spherical harmonics coefficients are established the source sound emissions for any combination of theta and phi can be calculated using the FLULA2 model (Butikofer, 2006).

The resulting FLULA2 propagation model based on spherical harmonics defined the directional spectral sound pressure level at a reference distance (Krebs, Butikofer, Pluss, & Thomann, 2003) (Krebs & Thomann, 2008). The directivity characteristics were represented as a sum of the spherical harmonic functions for each one-third octive band separatley.

$$L_k\ \left(r_{ref},\theta,\varphi\right) = \sum_{i=0}^{n}\ \sum_{m=-i}^{i} A_{k,i}^{m}\left(r_{ref}\right) Y_i^m(\theta,\varphi) \tag{4}$$

The sound level in the one-third octive band *k* is $L_k\ \left(r_{ref}, \theta, \varphi\right)$ where the reference distance is $r_{ref}$. Theta is the polar angle defined as the angle between the logitudinal axis of the flight direction and the direction from the aircraft to the observer. The azmuthal angle phi is measured in the x-y plane as shown in Fig. 8 below (Krebs W. , Butikofer, Pluss, & Thomann, 2003). The order of the spherical harmonics used is *n,* while the sperical harmonics are $Y_i^m(\theta, \varphi)$ and the coefficients are $A_{k,i}^m\left(r_{ref}\right)$as referenced earlier. The theta and phi coordinates indicate locations on a sphere and are also shown in Fig. 8. A well-established repository of fixed wing aircraft noise simulations completed using spherical harmonics in FLULA2 exists currently (Krebs W. , Butikofer, Pluss, & Thomann, 2003).

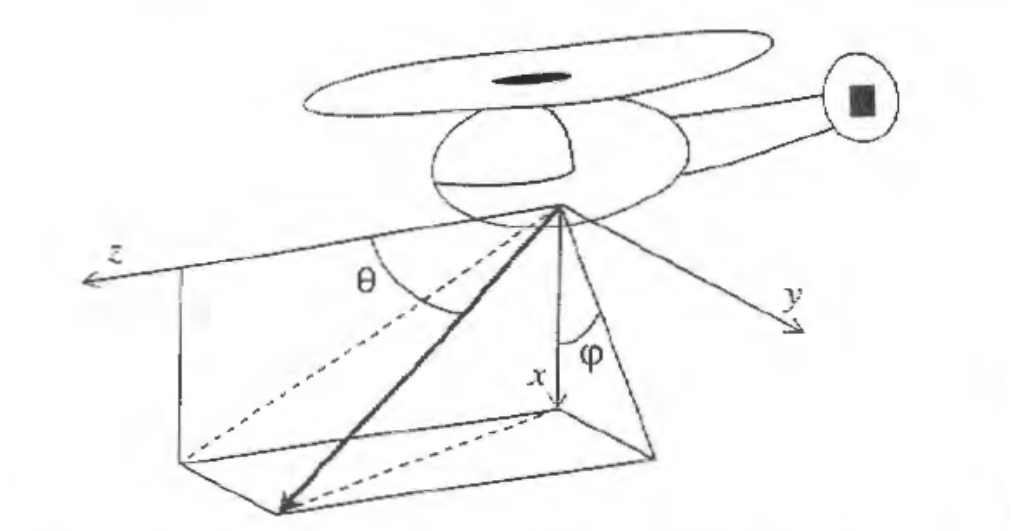


**Figure 8. Coordinate System Reference (Krebs W. , Butikofer, Pluss, & Thomann, 2003)**

The RNM and FLULA2 approaches account for and incorporate Doppler effects into their models because the source noise can be, and at times is traveling at high velocities beyond

MACH conditions. The source characterization presented in this thesis will be constructed with a static source and moving microphone. However the motion of the microphone will be performed by humans, therefore Doppler effects will not be present in the source representation. This must be kept in mind as the thesis proceeds and will be discussed in more detail in future sections because any comparison of the thesis measurements to the RNM or FLULA2 models will not include Doppler effects (G.P. Howell, 1986) (Piet, 2002).

### Static Source-Static Array

Thus far the techniques examined in detail were utilized when the noise source is dynamic and the array is static. As mentioned, it is the intent of this thesis to explore the measurement techniques for a static source and a dynamic array. However, before the author can fully begin to investigate this case, there is the case of static source and static array that must be explored.

#### Planar Near Field Acoustic Holography

Another method to construct an acoustic source directivity patter is Near-field holography. One Near-field Acoustic Holography (NAH) technique uses a planar array to capture the sound source data from a static source. The planar NAH technique begins with a static source and static array, but the planar two-dimensional array can then be moved to predetermine locations in the near-field around the source. The collection of these multiple static-static data collections is then used to model the acoustic source in its entirety with the holographic method (James, et al., 2011).

The three-dimensional sound field properties are then constructed from the holographic measurements captured from the two-dimensional rectangular array using the partial field decomposition (PFD) technique. PFD requires at a minimum the same numbers of reference microphones as there are independent, uncorrelated sources. In most applications of NAH this requirement is obtained by locating a reference microphone near each discrete source (James, et al., 2011). NAH creates the three-dimensional near-field sound volume by mapping the two-dimensional "hologram" measurement. Most often a two-dimensional measurement of the pressures in the source near-field will be used to construct the three-dimensional acoustic properties and quantities at the source (James, et al., 2011). This is not always the case as will be discussed in the next section dealing with the spherical NAH method.

It has been established that the situation will determine the number of microphones in the array for measurement in NAH (James, et al., 2011). For example, measuring a large static object such as a jet aircraft would require substantially more microphones on the two-dimensional, holographic, planar array then for a measurement on a typical household lawn mower. However, NAH techniques for planar arrays suggests that even though there is not an exact number of microphones for each situation, the best results come from a linear array extending far down the source. If PFD was to be performed in a situation where multiple sources are perfectly correlated then only one reference microphone is required. On the other hand, the number of reference microphones will equal the number of uncorrelated sources (James, et al., 2011).

### *Measurement array*

The microphones used in a planar NAH measurement of the United States Air Force F-22 jet aircraft performed by the Blue Ridge Research and Consulting (BRRC) team (comprised of Brigham Young University and The University of Alabama-Birmingham) under an Air Force Small Business Innovative Research (SBIR) grant were 6.35 mm G.R.SA.S type-1 pre-polarized microphones. The microphones were chosen because they had the ability to record sound pressure levels up to 173 dB and frequencies from 5 Hz to 30 kHz which was necessary to measure a full scale F-22 jet plume (James, et al., 2011). Because this NAH measurement was funded by the U.S. Government under a SBIR grant, there were specific restrictions placed on the number of microphones to be used in the array. Therefore, the planar array consisted of 90 of these microphone types and moved via four wheels and a guide rail along the jet plume (See Fig. 9). This array set up gave the BRRC team the ability to place the array at a near field location to the jet engine source and the use the following method (James, et al., 2011):

1) Turn on the engine source and let it stabilize for 30 seconds
2) Throttle the engine source at a desired power
3) Collect the engine source data via the planar array
4) Reduce engine power to idle state for “cool down” period
5) Reposition the planar array to a different, predetermined location in the near-field

6) Repeat process

"The measurements were repeated for four engine conditions ranging from idle to full afterburner, yielding over 6,000 measurement points and making this the largest near-field acoustic measurement of a high-powered military jet ever performed" (James, et al., 2011).

**Figure 9. Planar Array Constructed for a NAH Measurement (James, et al., 2011)**

This process is known as the "patch" holography measurement approach (James, et al., 2011). In this method of planar NAH, the source is not completely surrounded in three-dimensions by a measurement microphone array (James, et al., 2011). This static array-static source NAH patch measurement is a compellation of a number of static-static measurements. Table 1 is a sample of the array positioning during the F-22 NAH data collect done by BRRC.

**Table 1. Examples of Array Positions from F-22 NAH Data Collection (James, et al., 2011)**

| Run | Guide Rail Location Offset (m) | NAH Array Height (m) |
|---|---|---|
| **1** | 4.1 | 1.9 |
| **2** | 4.1 | 1.3 |
| **3** | 5.6 | 1.3 |
| **4** | 5.6 | 1.9 |
| **5** | 5.6 | 0.7 |
| **6** | 4.1 | 0.7 |
| **7** | 8.3 | 1.3 |
| **8** | 8.3 | 1.9 |
| **9** | 5.6 | 1.9 |
| **10** | 5.6 | 1.3 |

The height of the array was adjustable from roughly three feet to seven feet above the ground with the 90 microphones spaced six inches apart. This is considerably less than the FLULA2 and RNM "goal post" array styles with heights of 164 feet and 175 feet respectably. The array allowed for flexible placing of the microphones so that the spacing could be as close as two inches if needed. Traditional holography methods require microphone spacing to be no larger than half the wavelength of the highest frequency of interest. Anything closer than a half inch would affect the resolution due to a two measurement per wavelength restriction (James, et al., 2011).

### *Source noise directivity pattern construction*

Planar NAH utilizes algorithms to assign the fields to a propagation from the source with a method titled Statistically-Optimized Near-field Acoustical Holography (SONAH). SONAH dissects each partial field into a set of plane-wave functions. These functions are then

propagated to reconstruct the surface and determine the geometrical locations of the hologram (See Fig. 10). The use of NI LabVIEW software enabled visualization of the data monitoring and validation (James, et al., 2011).

**Figure 10. Measured SPL Map Overlaid on a F-22 Photo at the Approximate Location of Measurement (James, et al., 2011)**

## Spherical Near Field Acoustic Holography

The spherical NAH method is defined when the static sound source may be entirely enclosed by a spherical static array on which sound pressure is measured (Lee, 1996). This technique differs from the planar array NAH method because the spherical microphone array (SMA) provides the ability to capture and characterize three-dimensional sound source for volumetric intensity imaging. In this technique not only does the source remain static during the measurement process as in the planar method, but the array remains in the same location throughout the entire measurement process as well. The spherical array accounts for the sound

pressures at the receiver microphones in all planes and directions encompassing the source rather than just in parallel planes (Parthy, Jin, & Schaik, 2009).

**Figure 11. Dual, concentric 64 Microphone SMA with baffler (Parthy, Jin, & Schaik, 2009)**

### *Measurement array*

One spherical NAH method used a dual, concentric rigid and open SMA consisting of 64 microphones centered a radius of 1 meter from the center of the sphere (See Fig. 11). This array

construct has been shown to increase the available frequency range of analysis and can be used to recreate the three-dimensional noise source in the near field (Parthy, Jin, & Schaik, 2009). Each of the two concentric spherical arrays has 32 DPA type 4060-BM unidirectional microphones. The source signals were then recorded in MADI format onto a personal computer and a RME Hammerfall DSP MADI PCI sound card (Parthy, Jin, & Schaik, 2009).

### *Source noise directivity pattern construction*

In this spherical NAH arrangement there are two measurement surfaces comprised of the rigid and open concentric spherical microphone arrays. The intent of this method is to combine the measured data and NAH analysis from each of the concentric arrays and produce the three-dimensional holographic projection of the acoustic intensity field. Since the spherical coordinate system is separable, the holographic projection coefficients can be determined (Parthy, Jin, & Schaik, 2009). The projection coefficients $P_{mn}(k)$ are established as:

$$P_{mn}(k) = \sum_{j=1}^{M} \alpha_j \frac{p(kr,\Omega_j)}{b_n(kr,ka)} Y_n^{m*}(\Omega_j) \quad (5)$$

In Eqn. 5 we define (Parthy, Jin, & Schaik, 2009):

1) The wave number is $k$ and it is defined as $k = \frac{2\pi}{\lambda}$
2) λ is the wavelength
3) $r$ is the radius as which the SPL is measured
4) $a$ is the radius of the inner rigid spherical baffle where $a \leq r$

5) $\Omega_j$ is the angular position of microphone $j$ on the array in spherical coordinates

6) $M$ is the number of microphones on either array, therefore it is 32 in this case

7) $\alpha_j$ is a weight for each position related to the spherical sampling $\alpha_j = \frac{4\pi}{M}$

8) $p(kr, \Omega_j)$ is the pressure recorded at the microphone at position $\Omega_j$ on the array

9) $b_n(kr, ka)$ is a modal coefficient

10) $Y_n^m(\Omega_j)$ are the spherical harmonic functions which are defined in Eqn. 6 and were referenced earlier with the associated Legendre function $P_n^m$ as:

$$Y_n^m(\Omega) = Y_n^m(\theta, \varphi) = \sqrt{\frac{2n+1}{4\pi}\frac{(n-m)!}{(n+m)!}}\, P_n^m(\cos\theta) e^{im\varphi} \quad (6)$$

From Eqn. 5 and with the use of the spherical harmonics defined in Eqn. 6, the holograph projection coefficients can be determined. Once determined the coefficients can then be used to construct a single radius which is a combination of the two measurement arrays. The near field sound propagation can then be projected to this newly constructed radius. This is accomplished by use of Eqns. 7-10 (Parthy, Jin, & Schaik, 2009).

$$P(k\vec{r}, \Omega_o) = \sum_{n=1}^{N} P_{nm}(k) j_n(k\vec{r}) \sum_{m=-n}^{n} Y_n^m(\Omega_o) \quad (7)$$

$$v_r(k\vec{r}, \Omega_o) = \sum_{n=1}^{N} P_{mn}(k) \frac{j_n'(k\vec{r})}{-i\rho c} \sum_{m=-n}^{n} Y_n^m(\Omega_o) \quad (8)$$

$$v_\theta(k\vec{r},\Omega_o) = \sum_{n=1}^{N} P_{mn}(k) \frac{j_n(k\vec{r})}{-i\vec{r}^2 k\rho c} \sum_{m=-n}^{n} \frac{\partial Y_n^m(\Omega_o)}{\partial\theta} \quad (9)$$

$$v_\varphi(k\vec{r},\Omega_o) = \sum_{n=1}^{N} P_{mn}(k) \frac{j_n(k\vec{r})}{-i\vec{r}^2 (\sin\theta)^2 k\rho c} \sum_{m=-n}^{n} \frac{\partial Y_n^m(\Omega_o)}{\partial\varphi} \quad (10)$$

In Eqns. 7-10 it is necessary to now define,

1) $P(k\vec{r},\Omega_o)$ is the pressure
2) $v_r(k\vec{r},\Omega_o)$ is the radial velocity
3) $v_\theta(k\vec{r},\Omega_o)$ is the velocity in the theta direction
4) $v_\varphi(k\vec{r},\Omega_o)$ is the velocity in the phi direction
5) $\vec{r}$ is the projection radius
6) $\Omega_o$ is the projection angle in spherical coordinates
7) $\rho$ is the air density
8) $c$ is the speed of sound
9) $N$ is the truncation order for the Fourier-Bessel expansion

Figure 12 is an example of a holographic projection where the projection coefficients for the rigid and open arrays are yet to be combined. In contrast, Fig. 13 displays the combination projection of the open and rigid arrays along with the inner rigid array projection only.

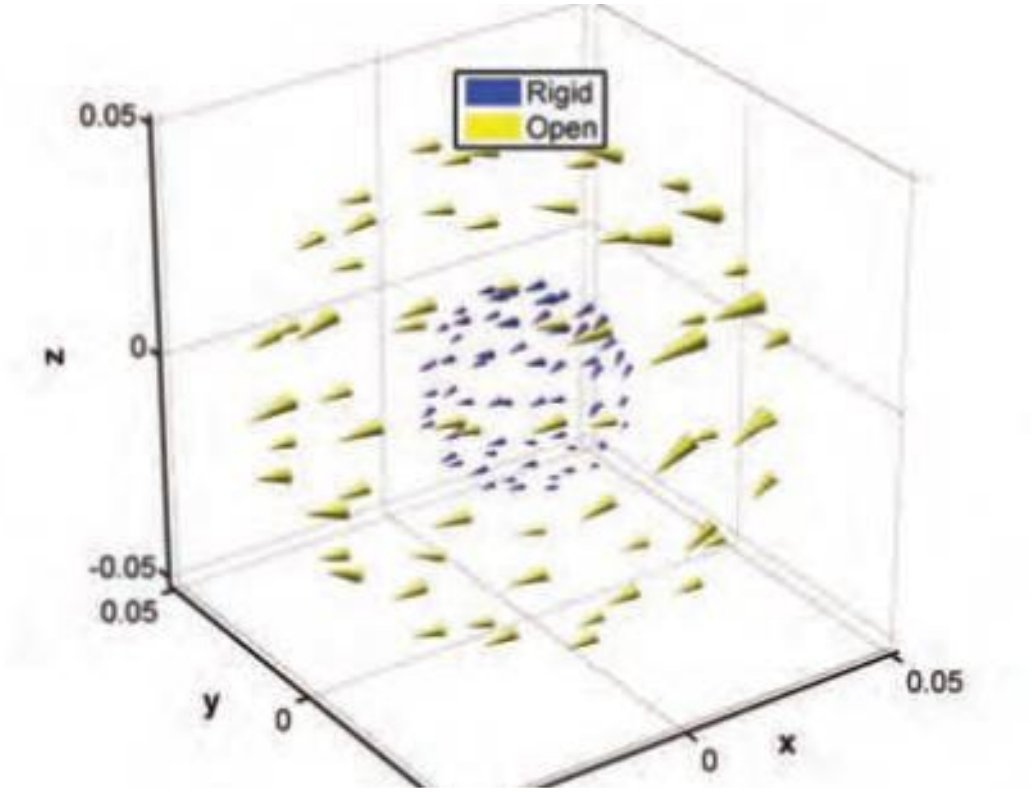


**Figure 12. Holographic Projection Example where Coefficients have not been combined (Parthy, Jin, & Schaik, 2009)**

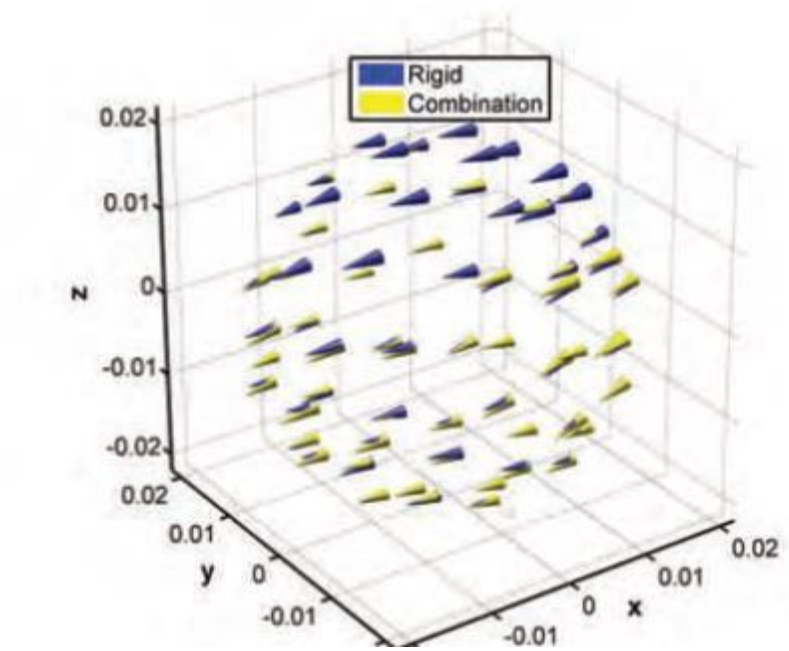


**Figure 13. Combination Projection and Rigid Projection (Parthy, Jin, & Schaik, 2009)**

Further exploration was done for the SMA NAH method. An estimation of the combination pressure field without the array present and no scattering from the rigid baffle was conducted at the 32 corresponding microphone locations. This estimate was established as the baseline measurement values (Parthy, Jin, & Schaik, 2009).

Next, the projection coefficients from the rigid array only and the open array only were used to estimate the pressure field at both measurement surfaces. Comparing the pressure estimates of both arrays separately with the combination projection estimate at 2850 Hz source and a 5000 Hz source demonstrated an advantage of the combination projection NAH technique in total relative error. Here, total relative error is defined as the absolute value of the error in

the pressure value divided by the pressure value (Parthy, Jin, & Schaik, 2009). The results are presented in Table 2.

The spherical holographic projection is conducted in a similar manor as the planar array case. However, the dual SMA approach to NAH improves the holographic projection of the acoustic intensity field by combining the coefficients of both concentric arrays to reduce relative error (Parthy, Jin, & Schaik, 2009).

| Frequency (Hz) | Rigid Array TRE | Open Array TRE | Combination TRE |
|---|---|---|---|
| 2800 | 86.3 | 184.01 | 15.58 |
| 5000 | 36.16 | 55.91 | 30.43 |

**Table 2. Total Relative Error (TRE) Pressure Field Estimates (Parthy, Jin, & Schaik, 2009)**

## Static Source – Manually Maneuvered Dynamic Array

In the remainder of this thesis the author will leverage the works above to select the microphone type, array construction, data collection techniques and software and validation methods as well as the data recording devices and experimental set up in order to measure a static sound source with a man portable dynamic array. In the remainder of this thesis when referring to a dynamic measurement or dynamic array the author is describing a lightweight microphone measurement array that was manually maneuvered around a static noise source. The author will also leverage the previously described methods and techniques in order to characterize the three-dimensional acoustic properties of a static source from a dynamic microphone array.

## III. METHODS

The methods chosen for this thesis reflect the careful consideration that was given to the software, hardware and facilities that were available. Both the hardware and software selections made for the measurement of a near-field noise directivity source were chosen for their technical capabilities as well as their cost effectiveness and availability. Similarly, the noise source and experimental set up were selected based on the desire to maximize available infrastructure and settings. The following section of this thesis details the experimental design and the procedures used for the acoustic data collection of a static source with a man portable dynamic microphone array.

### Experimental Design

The first measurements performed were conducted in an anechoic chamber at the Air Force Research Laboratory's Human Effectiveness Directorate. On the day the measurements were conducted the temperature conditions in the chamber were measured to be 64 degrees Fahrenheit and at a 64% humidity level. The measurement was performed with two individuals in order to maximize the straightforwardness when collecting data. Their roles are defined as:

1) Array Operator - During data collection this individual manually manipulated the location of the measurement microphone around the acoustic source.

2) Interface Operator – Responsible to coordinate what was being displayed on the laptop for the data collection with the array operator to ensure the

measurement was performed properly. During data collection this individual was located at the laptop to:

a) Start the application

b) Ensure that the system was operating correctly

c) Start the application data collect

d) Pause the application when and if necessary

e) Stop the application from collecting data

It should be noted that the data collection process could be configured in such a way as to allow one individual to perform a measurement.

The array was physically wired to a laptop at a location approximately 7 feet from the noise source as can be seen in Fig. 14. The entire anechoic chamber prior to measurements being made is also displayed in Fig. 14.

During the measurement a second stationary microphone was placed at a distance of 10 feet from the source. The data collected at this microphone was used as validation data in comparison with the dynamic microphone array data. The stationary validation microphone can be seen in Fig. 15. It was important that the validation microphone be placed a minimum of three and a half feet from the source as the data would later be normalized to a sphere of one meter (3.28 feet).

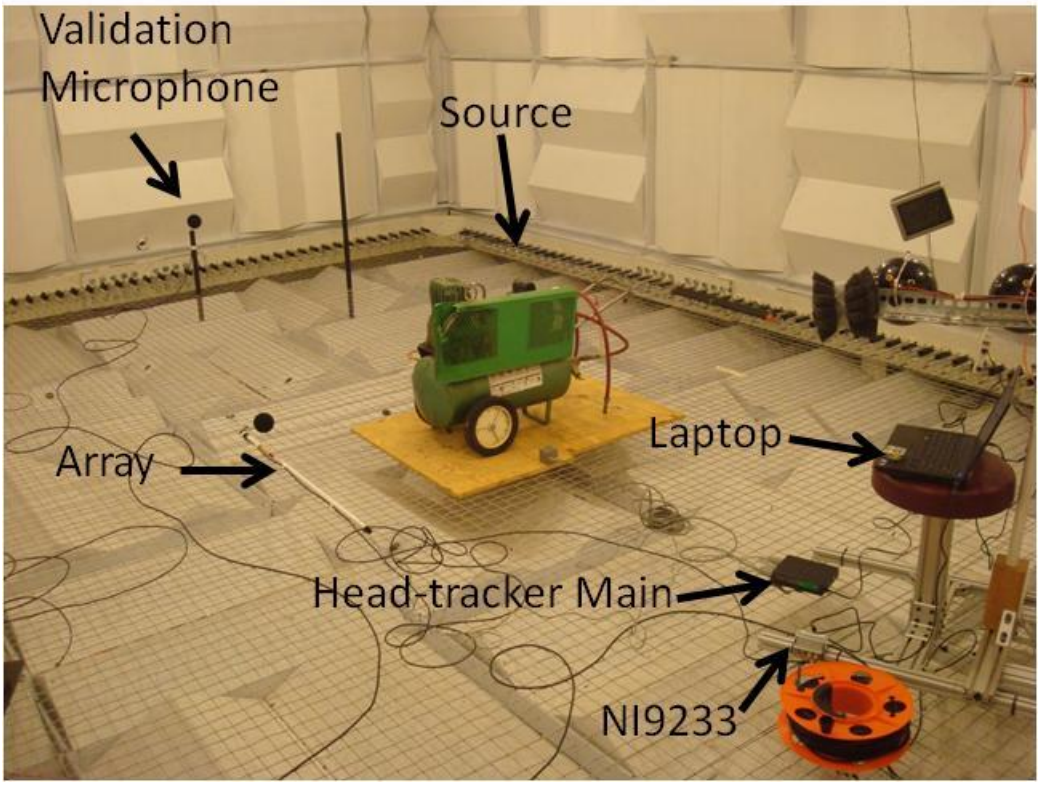


**Figure 14. Anechoic Chamber Measurement Setup**

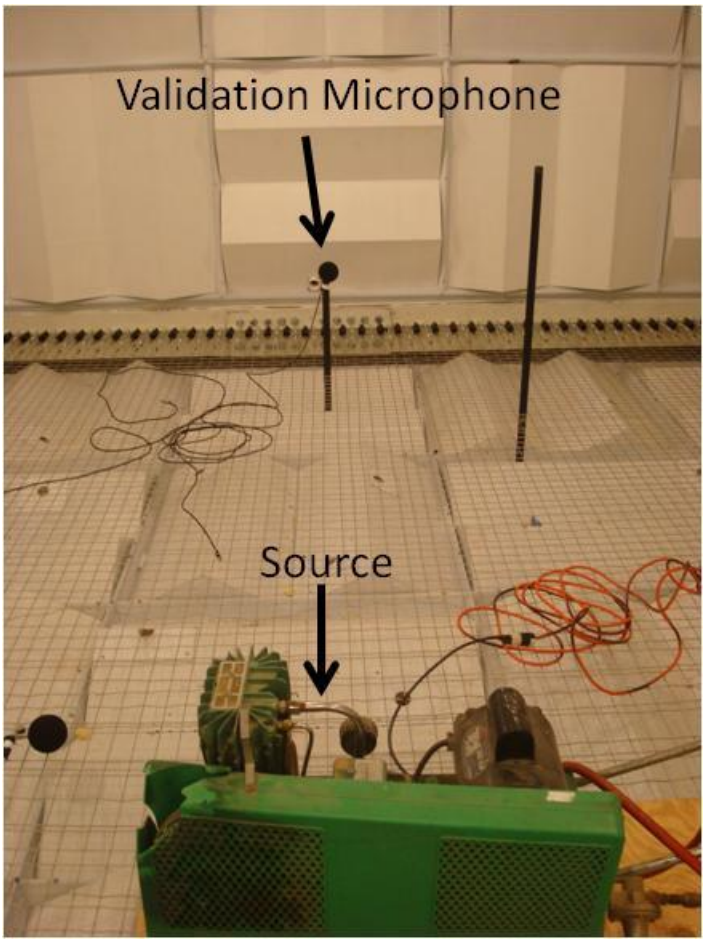


**Figure 15. Source and Stationary Validation Microphone**

## Instrumentation

Requirements of Data Collection

1) Setup time 15 minutes or less
2) Minimal auxiliary power
3) Maximum of two persons to operate
4) Able to be operated by one person if necessary
5) Lightweight, man-portable array

The acoustic measurement and validation data was collected using G.R.A.S. Sound and Vibration microphones type 46AO. These specific microphones were chosen because they did not require an external bias voltage source and they were of minimal size and weight. For this measurement the microphone power came from a constant current supplied via a USB connection to the laptop, a Dell Latitude E6410, through a four channel National Instruments NI9233 USB carrier to the microphones as depicted in Fig. 16.

Only two channels were used out of the four available, one for the measurement microphone and the other for the validation microphone. Also, the small size, 84mm, and lightweight nature, 33 grams, of the microphone made it a viable choice.


**Figure 16. G.R.A.S. Microphone and NI9233 USB Four Channel Carrier**

The array operator manually manipulated the array around the source to collect the data; therefore it was important that the size and weight of the microphones were considered. This addressed the lightweight requirement by ensuring that the operator was able to move the array in numerous locations around the source for extended periods of time if necessary without creating physical fatigue.

In order to capture the orientation of the dynamic measurement microphone to the noise source a head-tracker was used. The choice of head-tracker was limited by availability and connectivity. Therefore, a Polhemus Patriot head-tracker was the type used in this measurement. This particular head-tracker was composed of three main system components and can be seen in Fig. 17. Most common head-trackers require a RS-232 port for data transfer. The main unit was powered by an external A/C cord and connected to a laptop via USB interface.

Different from the microphone, the head-tracker required an external power source. The other two system components are the head-tracker source, or cube, and the sensor itself. The source cube was labeled with the x and y directions. The manufacturer's instructions explained that the z-direction is in the negative as see in Fig. 18.

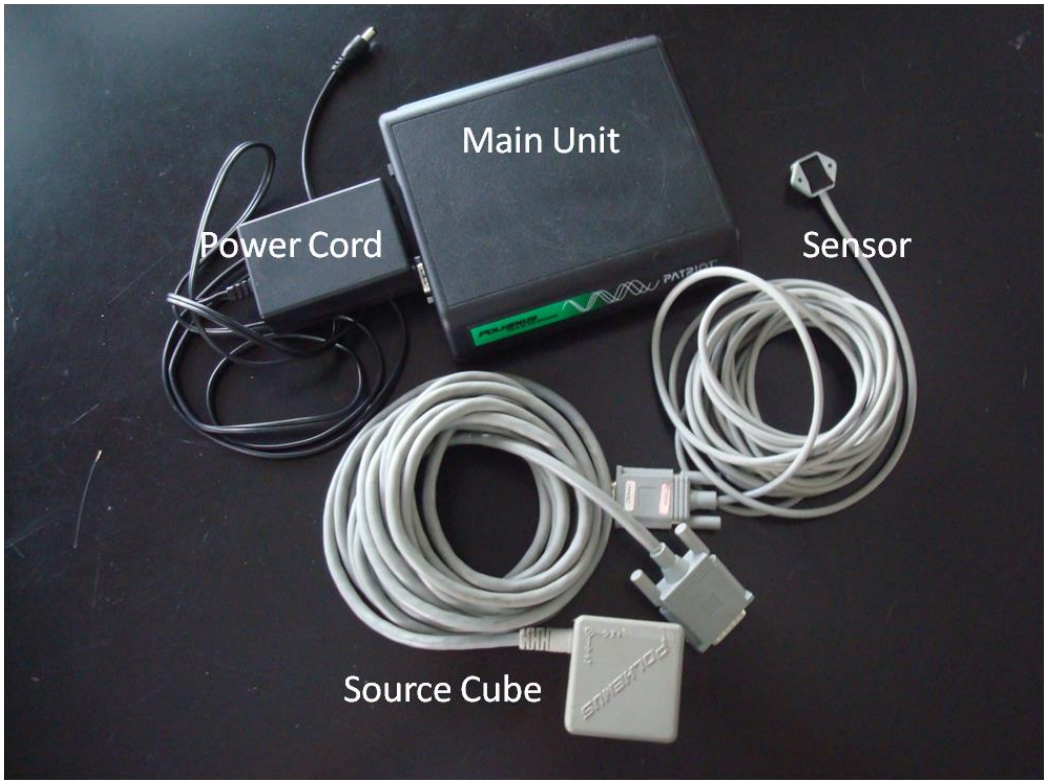


**Figure 17. Head-tracker Components**

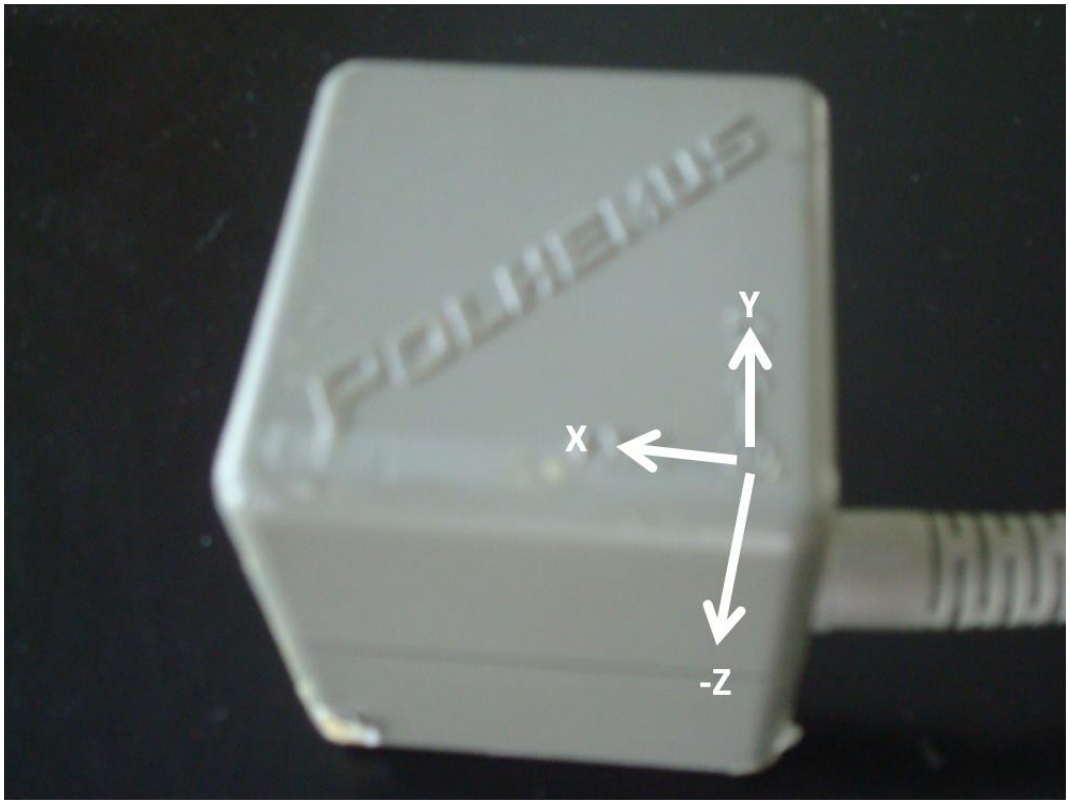


**Figure 18. Head-tracker Cube with Axis**

In order to display the location of the microphone relative to the noise source when measuring, the author chose the default position of the source cube to be fixed in the x-direction facing the noise source. The sensor portion of the head-tracker was placed on the array near the microphone as shown in Fig. 19. The entire assembled array with the G.R.A.S. microphone and the head-tracker sensor incorporated with a 5 foot dowel can be seen in Fig. 20.

**Figure 19. Array Microphone and Head-tracker Sensor**

The head-tracker yields data in the form of x, y and –z position as well as azimuth, elevation and roll in reference to the static source cube from the dynamic sensor. In this thesis

only the x, y and -z information was required to construct data spheres. This process will be addressed in detail below.

**Figure 20. Assembled array with the G.R.A.S. microphone and the head-tracker sensor incorporated with a 5 foot dowel.**

Unless any adjustment was made, the system assumes the source cube with the sensor on top of it as the coordinate center. In order to move the sensor a distance from the source cube and establish a new coordinate frame center, a boresite technique was required. This technique had to be accomplished prior to each measurement. The technique consisted of placing the sensor on or near the top of the noise source. With the sensor at this location, a

coordinate transformation established the coordinate frame center now at the top of the noise source rather than at the source cube. This was accomplished in the software written for the data collection using National Instruments LabVIEW. Details are provided in the Data Acquisition section below. This resulted in usable data being collected relative to the top of the noise source rather than relative to the source cube a fixed distance away.

The array was then connected to the laptop via the NI9233 acoustic channeled carrier and the head-tracker for the measurement setup as seen in Fig. 14. This hardware created the instrumentation for the physical measurement portion of the data collection.

**Source Construction**

The intent of this thesis measurement was to capture the Sound Pressure Level (SPL) directivity of a static source that would then be modeled with a spherical harmonic technique. Careful consideration was given to the selection of the noise source for this thesis measurement. Sources that provided uniform or little sound directivity were excluded. This was acceptable merely as a preference by the author based on an opinion that ensuring the directivity of the source would be more interesting to study than a uniform directivity source.

Sources that had the ability to maintain an uninfluenced directivity at a maximum level without operator manipulation verses a noise source that required manipulation were determined to be relevant considerations. The experimental design explained above requires two operators. The addition of a third person would be required if the source had to be manipulated to achieve and maintain a maximum level. If the source noise required

manipulation in order to increase, decrease or fluctuate the level during the measurement it was not considered.

The intent of this measurement was to identify a stabilized, independent source that did not rely on any external manipulation to radiate a SPL at a maximum level. The data collection of a static noise source with all the equipment and software functioning properly for both measured and validated data was required in order to meet the intention of this thesis. Therefore considerations were made when selecting a noise source such as the size of the noise source object in length, height and width. It was the author's intention that the array would be able to be manipulated around and above the source without the operators having to use any external support to place the array above or around the source.

The head-tracker was limited by a functionality radius of 5 feet and this was taken into account when selecting the source size as to not exceed the capability of the head-tracker. The cables used were standard Belden 9223 low noise coaxial 50 Ohm and Delco Wire and Cable RG 58C/U cables. At a minimum, the cable length had to allow the array operator the ability to walk around half the source and measure a half- hemisphere of data. Then the procedure could be paused while the operator re-located to the other side of the source and a second half-hemisphere could be recorded. The size of the sources considered had to fit the constraints of the length of available cabling.

Therefore, based on these considerations a Sears brand 100psi twin-cylinder air compressor was chosen to be the static noise source that would be measured. The compressor details are found in Fig. 21. The dimensions of the compressor are as follows:

1) 29 inches in height
2) 28 inches in length
3) 19 inches in width

**Data Acquisition Software Design**

In addition to the measurement design and instrumentation in the above sections, the author chose to use National Instruments (NI) Laboratory Virtual Instrument Engineering Workstation (LabVIEW) as the programming language for the data acquisition of this thesis. "Because LabVIEW is a graphical programming language, it is often quicker to develop than using a text-based language and its programs are often more robust" (Mihura, 2001). Data acquisition is fundamental to many LabVIEW applications and NI manufactures a variety of data acquisition devices (Mihura, 2001).

In order to acquire, analyze and present the data in LabVIEW two block diagrams were constructed individually and then combined into one acquisition program. The first was for the head tracker data acquisition and the second was for the acoustic data acquisition. This approach allowed for simplicity when creating the data acquisition software. It enabled the creator to initially focus on software for acquiring data from each device without concern for the other before integrating them.


**Figure 21. Air Compressor Model and Information Sticker**

Figure 22 reveals the LabVIEW block diagram for the head tracker acquisition alone. Figure 23 shows the acoustic acquisition block diagram for dual microphones alone. The combination of the head tracker and acoustic block diagrams into a robust data acquisition software program is then seen in the Fig. 24 block diagram. In order to combine the two block diagrams as seen in Fig. 24 two "while" loops had to be inserted to enable the reading of the head tracker software at the same time as reading the acoustic acquisition software.

The interface needed to perform the measurement was constructed to be interactive and designed in a way that binary controls and indicators could be used to perform the tasks and status validations. It was necessary to be an intuitive interface design that any user that would be assisting the array operator in the data collection could perform the required tasks with little to no training or explanation. LabVIEW provided the ability to create an interactive instrument panel that allowed for these parameters.

The panel was designed for all the input and status information to be displayed on the left side and the remaining space was utilized for real-time monitoring and visualization as seen in Fig. 25. The operations were intended to flow from left to right and top to bottom of the panel. The information from the top left side of the panel to the bottom left side provided the user with all the necessary input and status information to complete a data acquisition set. The top left provided the input channels to be selected from a dropdown menu. Two channels were needed, one for the microphone that was being used for the measurement and one for the microphone that was used for the validation.

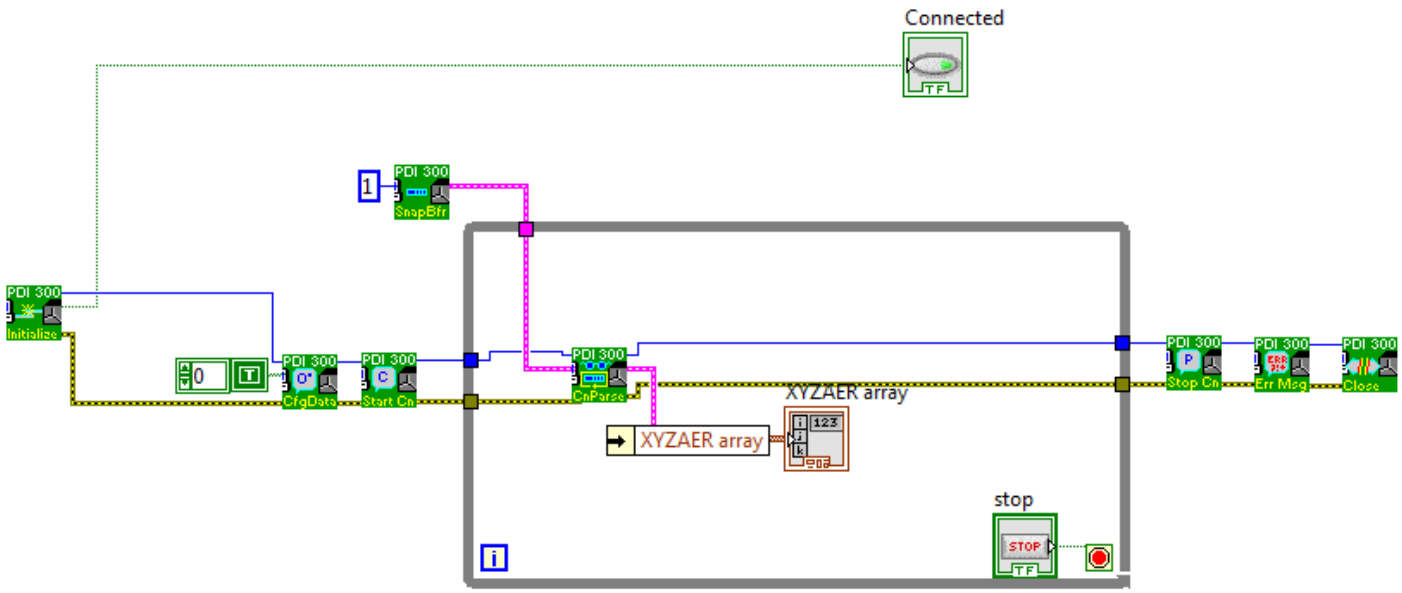


**Figure 22. NI LabVIEW Block Diagram for Head Tracker Data Acquisition Only**

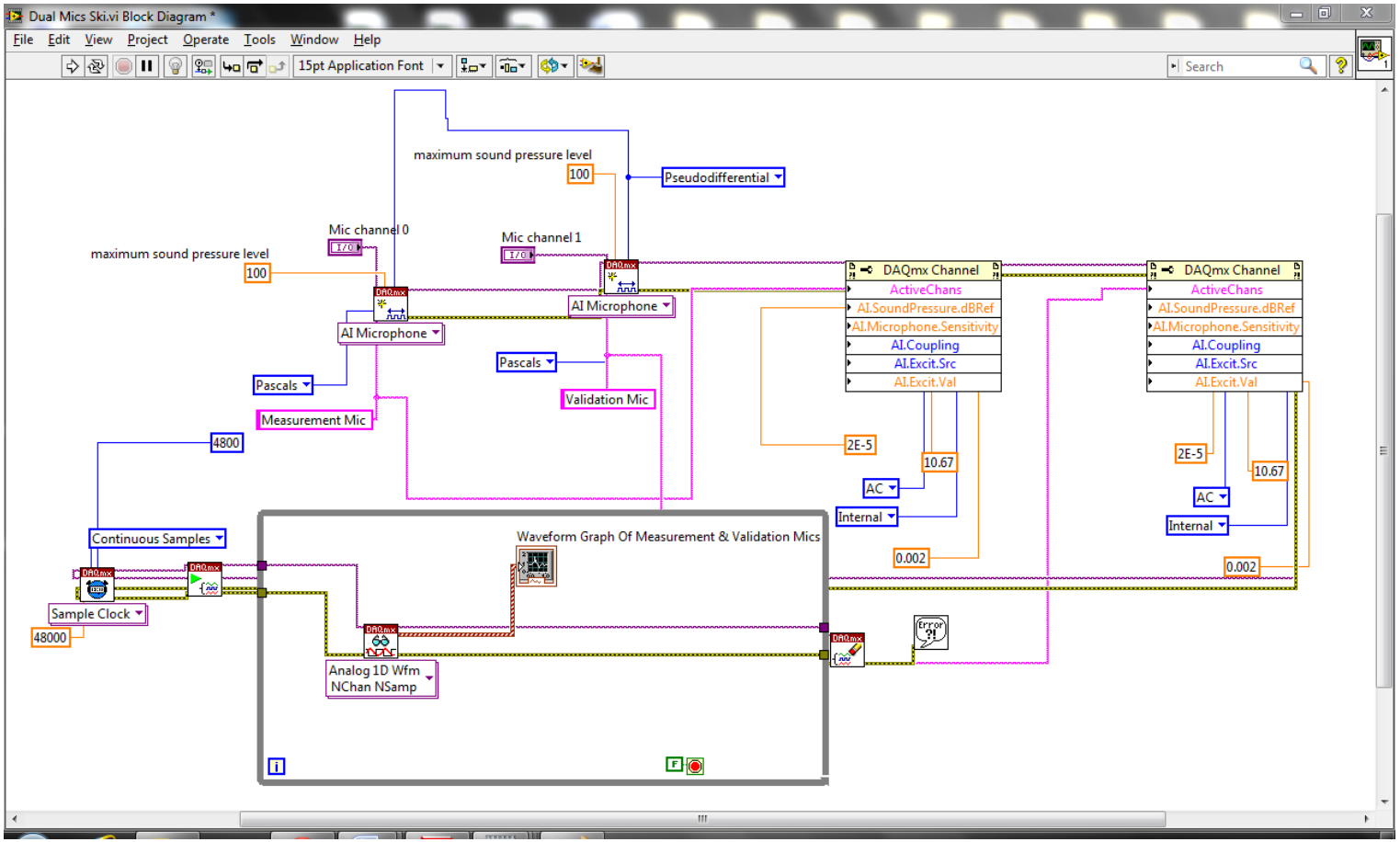


**Figure 23. NI LabVIEW Block Diagram for Acoustic Data Acquisition Only**

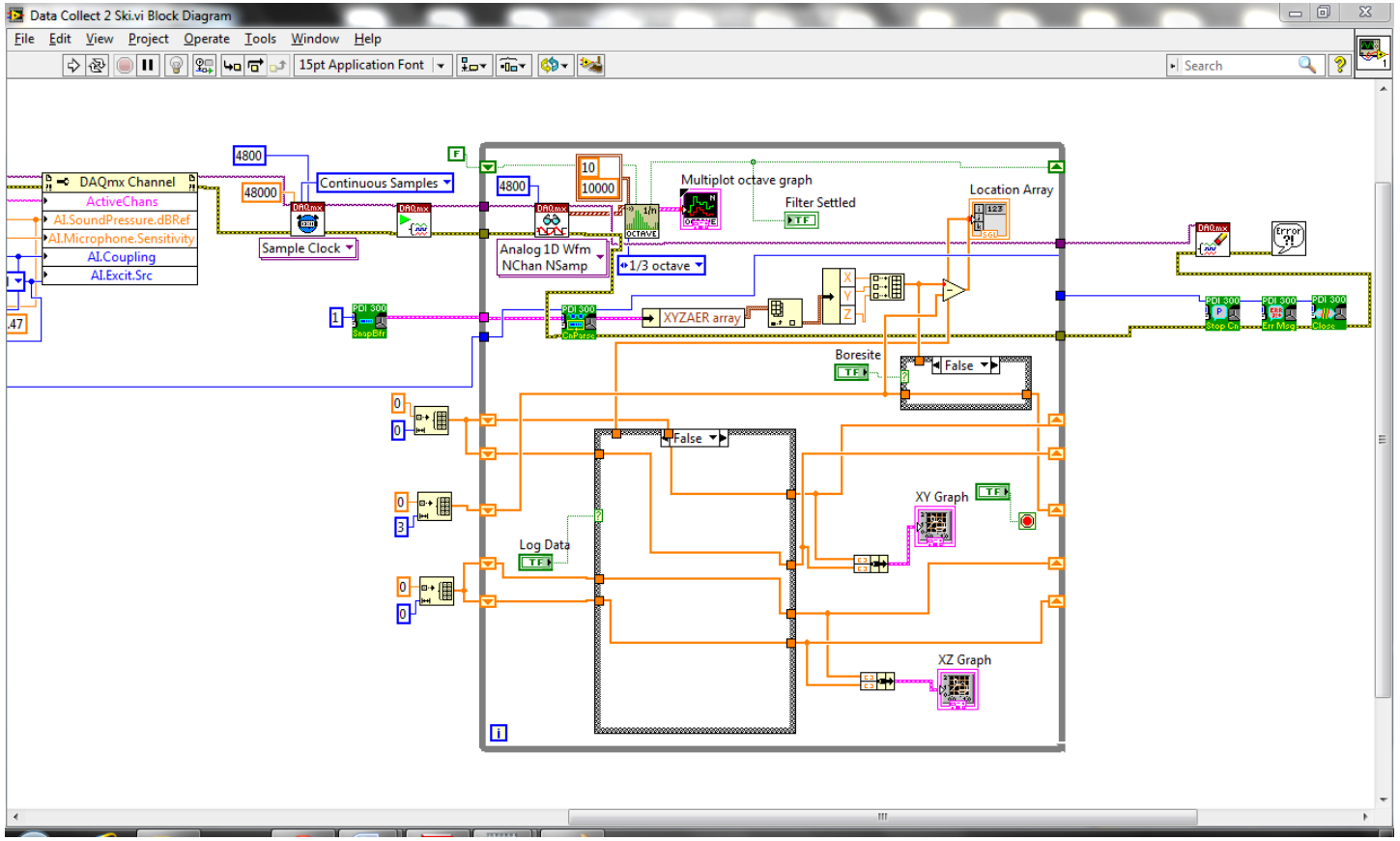


**Figure 24. NI LabVIEW Acoustic and Headtracker Data Acquisition Program Block Diagram.**

As seen in Fig. 25 channel zero was selected as the measurement or data collection microphone while channel one was chosen as the validation microphone channel.

The data collected was written onto Excel files. The paths for the collection of both the measured source data and the validation data are identified next on the front panel of the interface when moving toward the bottom left corner. This is completed by choosing the file path location previously decided upon for raw data storage. In this measurement the folder was located on the desktop. There was no preference used in selecting the paths for this thesis.

After the initial step of channel and file path selection was complete, the user was to select the "Run" arrow on the LabVIEW panel which is the standard start operation in any Lab VIEW data acquisition application. This caused the system to initialize and the user then worked down from the top left moving to the bottom left completing the following tasks in order:

1) Confirm head tracker connection status
2) Confirm filter settling
3) Boresite

With the display of a color, binary indicator the user was alerted that the status of the head tracker had gone from not connected to connected. Similarly, the operator would notice the same type of indicator for the filter settling activity once it was complete.

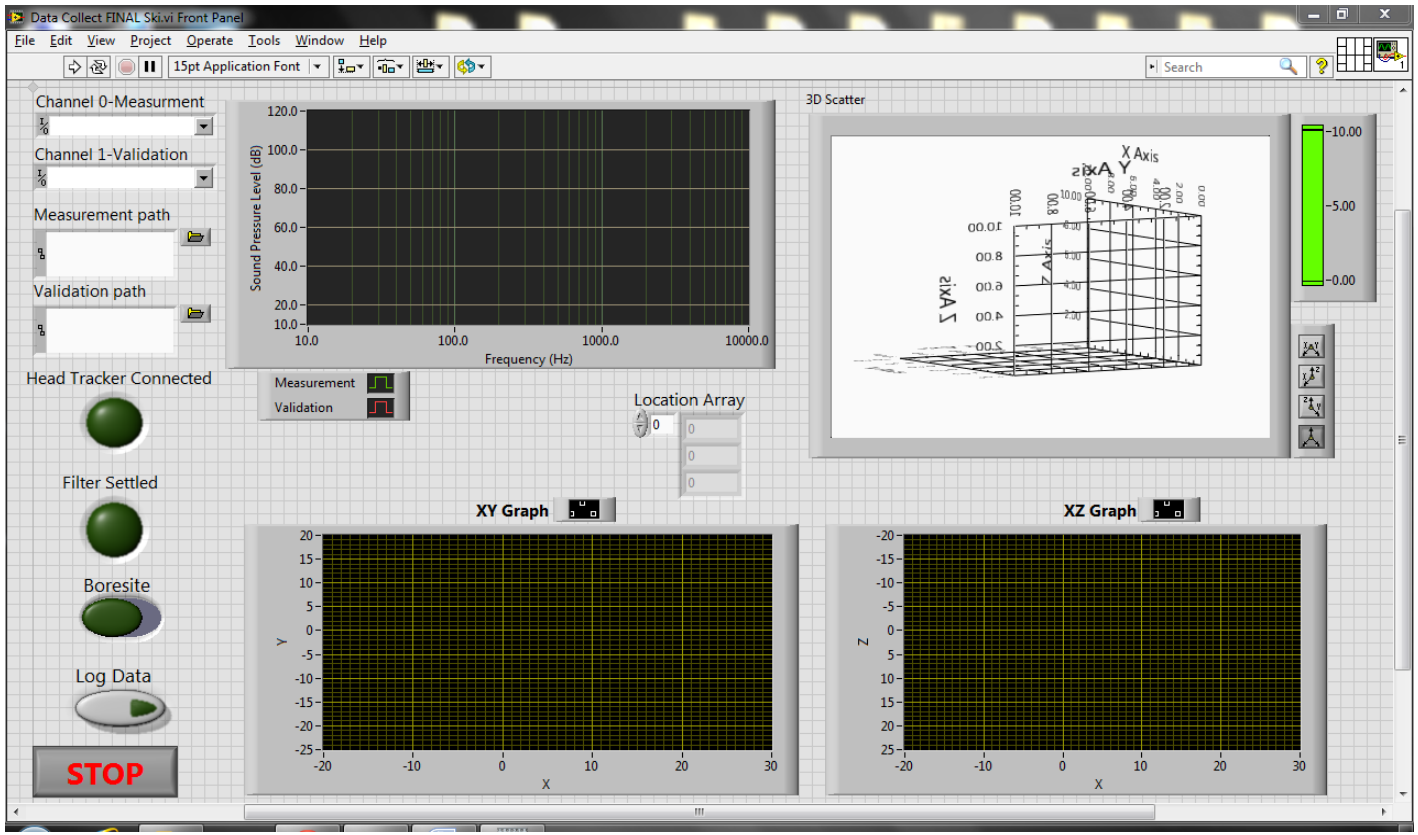


**Figure 25. LabVIEW Front Panel for Data Acquisition.**

Boresiting is the first time the user is required to manipulate a control that affects the physical hardware of the measurement system. By selecting the boresite control to an indication that it is engaged and then disengaging it approximately 15 seconds later the boresite task is completed. This is accomplished only when the array operator has placed the head-tracker sensor on top of or near the center/top of the source as described previously.

The interface operator is now able to announce to the array operator that all the produces are complete and the system is ready to collect data on the array operators command. Once this command is given, the user selects the control labeled “Log Data” to begin data collection. The remaining portion of the panel is designed to be able to monitor the data collection in real-time.

### Data Acquisition

Before the software could be considered complete for this thesis measurement the ability to collect data had to be verified. In order to determine if the data acquisition software was functioning properly an initial, crude data collect was conducted. The source was a 13 by 15 inch LG series 5212 television set with a built in DVD player. A DVD was installed into the player and the volume was set to a seven out of a maximum of 15 for this device. The setup is depicted in Fig. 26.

**Figure 26. Data Collection Software Functionality Test Set Up**

Since this was a preliminary trial to ensure functionality, there was no validation microphone and there was no array. The author simply held the head tracker at the base of the microphone as in Fig. 27. The head tracker source cube was placed approximately 13 inches from the television and was aligned so the x-direction faced the television as was the default position determined by the author. It was also centered on the television as can also be seen in Fig. 27. The result identified that the system was able to acquire data around the television.

**Figure 27. Microphone and Head Tracker Set Up for Functionality Test**

Once the system was deemed functioning the anechoic chamber measurement of the air compressor was conducted as seen in Fig 28. Six unique data collections occurred with the following distinctions:

1) First Collection-While maneuvering the array around the compressor the cords trailing the array displaced the head-tracker source cube thus causing the x-direction to be compromised. Additionally the compressor failed during the collection and at that point the collection was stopped.
2) Second Collection-The array operator remained stationary and was able to manipulate the array around all sides and the top of the compressor while remaining at a fixed location.
3) Third Collection-The array operator and the interface operator switched tasks.
4) Fourth Collection-The head-tracker source cube was relocated to a position of 24 inches to the center of the compressor. This was done because the real-time data displayed unaccounted for "holes" in the collection. It was thought that by moving the source cube closer to the source this anomalous data would be rectified.
5) Fifth Collection-The remedy in the fourth collection was successful. However, the real-time display yielded not enough data being collected on the top of the compressor.

6) Sixth Collection-A complete collection was conducted but with an emphasis on the top of the compressor. This was done by moving slower over the top to ensure a good collection.

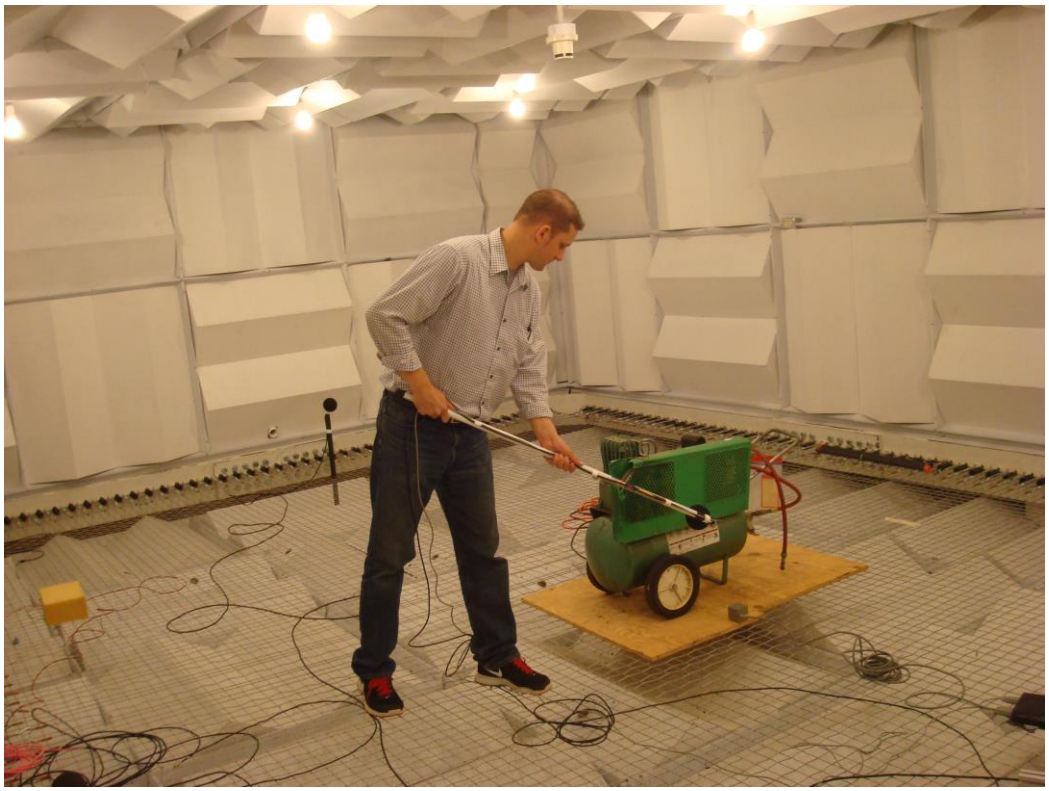

**Figure 28. Array Operator Conducting Data Collection**

The initial exploration of the data from this collection disclosed that the electromagnetic properties of the head-tracker source cube were corrupted by the placement on the metal

flooring of the chamber. Thus, this data collection was deemed unusable and a second measurement was initiated in a different location.

Located not in an anechoic chamber a second measurement was conducted in a room that would not interfere with the head-tracker. The room was susceptible to reverberation; however, those effects were negligible because the measurement microphone was inches away from the source. It was important to ensure the microphone remained in a position to maximize the acoustic collection from the source during measurement. Any reflections that were captured during the collection were determined to be acceptable as this location gave the ability to control the electromagnetic environment thus leading to a useable data collection. While the room did not contribute to any electromagnetic interference it is possible that the placement of the source cube in close proximity to a metal compressor along with the compressor being located in between the source cube and sensor at times during measurement may contribute to inaccuracies in the location data collected. It is also beyond the scope of this thesis to address the removal of any refection captured. This second data collection set up can be seen in Figs. 29-30. The distance from the compressor to the validation microphone remained at ten feet as in the first collection.

An outdoor location was considered for the second measurement. However, the best location that could be determined would make the collection susceptible to natural atmospheric conditions such as wind. Also present would be the presence of traffic sounds from the adjacent street. Finally, the outdoor location was abandoned because the occasion was close to

two major air conditioning units that would have provided a constant background noise source when they were running.

**Figure 29. Second Data Collection Set Up**

**Figure 30. Second Collection with Validation Microphone**

## Data Acquisition Technique

The collections all began with the array operator giving the command to begin the data collection. The array operator then started by using a "tooth brushing" method to collect the data around the compressor. This method was to manually move the array vertically from as close to the ground as possible to at least six inches above the height of the compressor and at as close to a horizontal constant distance from the compressor as could be obtained. The array was then moved back down to as close to the ground as possible. This procedure was repeated as the array operator walked slowly around the compressor always attempting to keep the array as close to a constant horizontal distance from the source. In the second collection the array operator remained fixed while using the "tooth brushing" technique around the sides of the compressor.

The array operator began at the front of the compressor with the array positioned roughly at the center of the compressor. Upon announcing to begin the data collection and receiving from the interface operator the confirmation that the system was ready, the array operator walked counterclockwise around the source utilizing the "tooth brushing" method until completing one revolution around the source and reaching the starting position.

The number of revolutions around the compressor was dictated by a scatter plot of data being built up in real time on the display and objectively determining that a robust amount of data around the source was collected. The real time scatter plot build up example can be seen in Fig. 31.

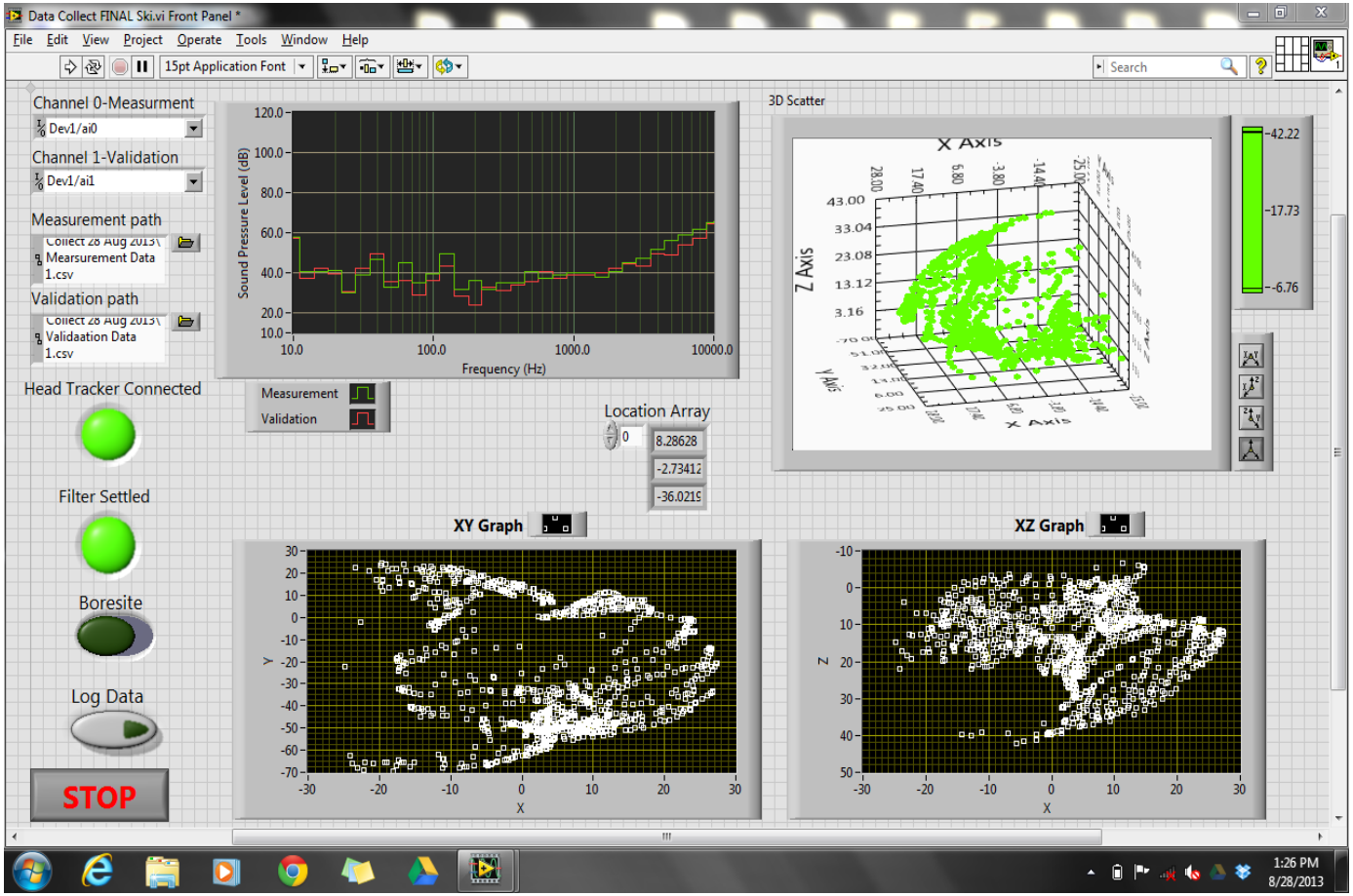


**Figure 31. Real-time Feedback Visualization Panel**

After the data around the sides of the compressor was collected, it was necessary to collect the data above the source. In order to complete this an “arching” method was employed. This consisted of the array operator positioning the array as close to the ground as possible and at least six inches in front of the compressor and to the right side of the compressor.

The array operator would then trace with the array a semi-circle at as close to a fixed radius from the center of the compressor as manually possible ending on the left side of the compressor. This motion was repeated back to the right side of the source. The array operator would continue this “arching” procedure while slowly walking from the front of the source to the back and would continue at least six inches beyond the back of the source. This was also conducted from the operator’s static position in the second measurement. By sweeping the “arching” array over the top of the compressor from front to back locations, the data above the source was able to be collected. Similar to the data collection around the sides of the compressor, the interface operator would examine the display in real time to ensure a sufficient amount of data above the source was collected. One additional collection method for above the compressor was a planar technique where the operator simply moved the array at as close to a fixed distance from the compressor from front to back while remaining stationary. The “arching” technique could also be conducted from front to back rather than side to side of the compressor. At all times during the collection, regardless of the technique, the microphone was pointed toward the source.

Once the “tooth brushing” and “arching” procedures collected a sufficient amount of data reviling a hemisphere type of shape surrounding the compressor position the “Stop” control was engaged and the data collection was complete.

During the collections there was never a need to pause the operation at any time. Once started, the transition from the “tooth brushing” technique to the “arching” technique was seamless. However, the software was created in such a way as to allow for this operation if it had been necessary. To invoke a pause in collecting data the array operator would announce that a pause was necessary. Upon receiving that command the interface operator would engage the “Log Data” control. The software would temporarily suspend that data collection until re-engaged. The array operator would notify the interface operator when the data collection was ready to proceed and at that time the “Log Data” control would be engaged again and the data collection would resume.

The importance of real time monitoring and visualization of the data enables the disclosure if a specific portion around the compressor was not collecting enough data. When this would occur as in the case of the fifth collection, it was immediately determined and that area could then be addressed by conducting another measurement with the guidance of the interface operator. Additionally, the pause feature could have been used once the “arching” and “tooth brushing” were complete to analyze the scatter plot and then re-engage the collection addressing any deficient areas. Real-time feedback also verifies the microphones are properly functioning by visualizing on the panel the SPL. The ability to visualize the data in real-

time with a pause function enables results to be viewed and validated as they are being collected. By presenting the SPL and real-time visualization on the panel this ensures that the data being collected is of good quality and quantity.

## Analysis

Once the software for the data collection was determined to be functioning properly and the second data collection of the compressor was complete, the next step was to engage further LabVIEW applications in order to model the collected data into a point cloud representing the compressor noise source directivity pattern. The spherical coordinate system depicted in Fig. 32 is used for this thesis.

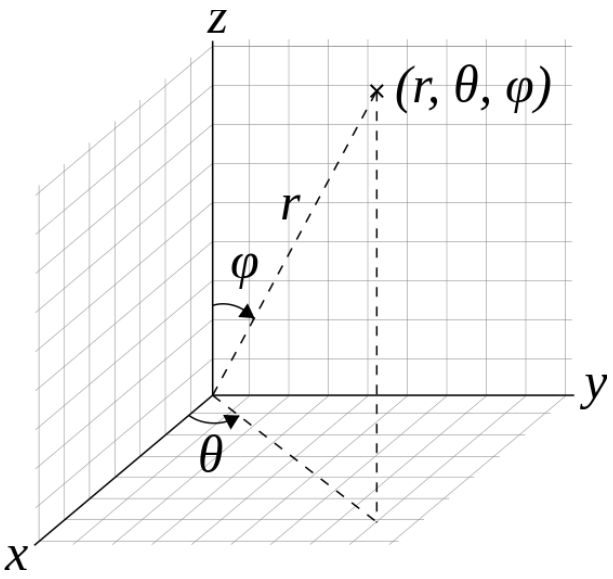


**Figure 32. Spherical Coordinate System Used in this Thesis**

To accomplish the point cloud model, the following steps were taken:

1) Read the raw data file

2) Convert from Cartesian to spherical coordinates

3) Convert from inches to meters

4) Normalize the radius to one meter

5) Correct Sound Pressure Level (SPL)

The Excel document that contained the measured data collected consisted of head-tracker x, y and z positions, the 31 accepted frequencies of the one-third octave band and the SPL at each position and frequency. In order to begin building a spherical representation with this data it was necessary to convert from Cartesian to spherical coordinates. This resulted in the position now being available in a radius and theta and phi angles (See Eqn. 4). The units of the Cartesian coordinates collected were in inches. Therefore, at this point in the procedure the radius remained in inches while theta and phi were in radians. Throughout this process the frequencies remain in Hertz.

$$(x, y, z) \rightarrow (r, \theta, \varphi) \tag{4}$$

Because the distance from the center of the compressor to the measurement array was not fixed during the measurement it is now necessary to normalize the measured radius. A one meter radius was chosen because this is the industry standard distribution (Devries, 1990)used to determine SPLs for hardware or appliances. It was also necessary to choose a normalization value in order to use spherical harmonics as will be discussed further.

The next step in the modeling software was to change the units of the radius from inches to meters and normalize to one meter. During this step the SPL was corrected to approximate the loss of energy from the measurement location to one meter. This was

accomplished by adding the losses due to the propagation from the measured radius to the one meter radius.

Recall that due to the completeness property of the spherical harmonics, any function $f(\theta, \varphi)$ evaluated on a spherical surface is expanded into a double series of spherical harmonics as referenced in Eqns. 5-6 (Jackson, 1999) (Arfken & Webber, 2001).

$$f(\theta, \varphi) = \sum_{l=0}^{\infty} \sum_{m=-l}^{l} A_{lm} Y_{lm}(\theta, \varphi) \tag{5}$$

where the unknown coefiicients, $A_{lm}$, are then defined as:

$$A_{lm} = \int d\Omega \, Y_{lm}^{*}(\theta, \varphi) f(\theta, \varphi) \tag{6}$$

Therefore, a regular/normal surface is required in order to use the properties of spherical harmonics as described in Eqns. 5-6. Since the head tracker data was collected in Cartesian coordinates a regular/normal function is defined in terms of Cartesian coordinates on the surface of the sphere at one meter. Then there is no radial dependence on the surface of the sphere and the coordinates are defines as follows:

$$\begin{aligned} x &= SPL \cos\theta \sin\varphi \\ y &= SPL \sin\theta \sin\varphi \\ z &= SPL \cos\theta \end{aligned}$$

Now the function on the surface of the sphere can be represented as

$$f(x, y, z) = f(\theta, \varphi) = \sum_{l=0}^{\infty} \sum_{m=-l}^{l} A_{lm} Y_{lm}(\theta, \varphi) \tag{7}$$

In matrix form this becomes:

$$\underline{F} = \underline{Y}\,\underline{A} \tag{8}$$

$$Y^{+}\underline{F} = Y^{+}\underline{Y}\,\underline{A} \tag{9}$$

$$\underline{A} = (Y^{+}Y)^{-1}\,Y^{+}\underline{F} \tag{10}$$

Eqn. 10 determines the coefficients where $\underline{F}$is the $(x, y, z)$ SPL at one meter. This process is repeated for each of the 31 frequencies and summed to form the measured sphere.

Recalling the Rotorcraft Noise Model (RNM) technique, the measured SPL is defined as $L_m$:

$$L_m = L_s - \sigma_{Divergent} - \sigma_{AA} - \sigma_{Ground\ Ref.} - \sigma_{Terrain} - \sigma_{Turbulance} - \sigma_{Other} \tag{11}$$

here $L_s$ is the predicted source level and is defined as :

$$L_s(\theta, \varphi) = \sum_{l=0}^{\infty} \sum_{m=-l}^{l} A_{lm}\, Y_{lm}\,(\theta, \varphi) \tag{12}$$

Exploring the remaining terms in Eqn. 11 reveails:

1) $\sigma_{Divergent}$ is defined as $20\,log_{10}\left(\frac{raduis\ (r)}{Distance\ Propagated}\right)$ (13)
2) $\sigma_{AA}$ is the atmospheric absorption standard according to the American National Standards Institute (ANSI)
3) $\sigma_{Ground\ Ref.}$ is the ground reflection
4) $\sigma_{Terrain}$ is the effects of the terrain
5) $\sigma_{Turbulance}$ is the effect of turbulence
6) $\sigma_{Other}$ are the other effects on the measured source

This measurement was conducted indoors at a close proximity to the source. Therefore the atmospheric absorption effect is not applicable in the calculation. Because the source was on

the ground rather than in the air and the measurement was conducted at a close proximity to the source, the effect of ground reflections is also not applicable to the calculation. Similarity, terrain and turbulence were not present and could also be eliminated from the calculation. The other effects on the measured source are not specifically defined, thus correcting for them is out of the scope of this thesis and they were able to be eliminated from the calculation. Thus the frequency dependent predicted SPL is defined as $L_p$ by:

$$L_p = L_s + 20\log_{10}\left(\frac{r}{Distance\ Propagated}\right) \quad (14)$$

Here the radius is the normalized one meter and the distance propagated is two meters. Therefore Eqn. 14 becomes:

$$L_p = L_s + 20\log_{10}\left(\frac{1m}{2m}\right) = L_s\text{+-}6 \quad (15)$$

The software enabled the collection of acoustic SPL data on a static source while the array operator manually manipulated a microphone array around that source. The data collected could then be used to determine the spherical harmonic coefficients thus leading to the acoustical modeling of the source measurement, prediction levels and validation technique as will be seen in the next section.

## IV. Data

The previous section concluded with the process used in LabVIEW to model the collected data into a point cloud representing the compressor noise source directivity pattern. The following figures present the LabVIEW software front panel output displays from the measurement effort in the non-anechoic room with the selected air compressor as previously described. Figure 33(a) represents the three-dimensional scatter plot of the Sound Pressure Level (SPL) data measured from the array after it has been normalized to one meter. The predicted scatter plot in Fig. 33(b) represents the predicted SPL at a one meter distance from the source also for spherical harmonic order five.

(a) (b)

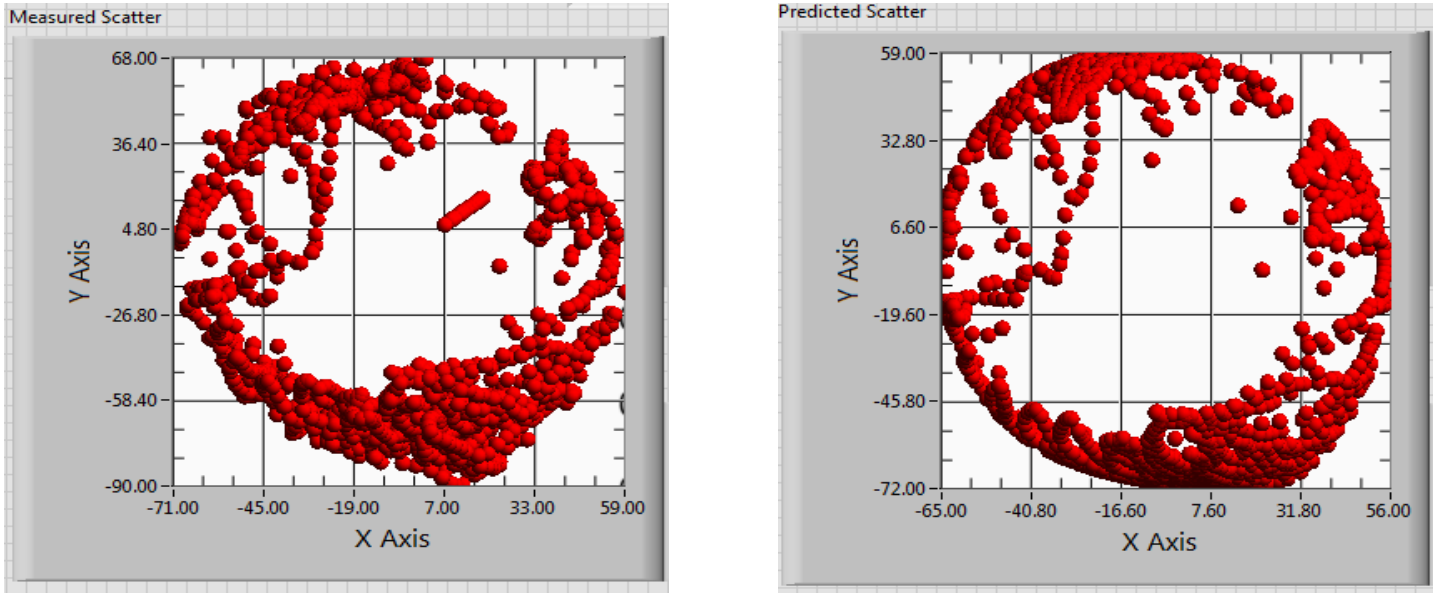


**Figure 33. Three-dimensional scatter plots of (a) measured and (b) predicted source noise directivity pattern at a normalized distance of one meter and spherical harmonic order of five.**

Figure 34 uses a waveform representation that depicts the measured and predicted data collection from the entire acquisition effort in the non-anechoic room on a single chart for spherical harmonic order five. This figure was also created by the LabVIEW software and displayed on the front panel with the scatter plots. This technique enables visualization of both measured and predicted data over the entire spectrum for analysis. It provides a qualitative examination of the relationship between the measured and predicted data.


**Figure 34. Waveform graph depicting the measured (red) and predicted (white) spectrum acquired over the entire measurement and computed for spherical harmonic order five.**

The scatter plots and waveform figures presented above were all obtained with a spherical harmonic order of five. The customized LabVIEW software application was built in such a way that the order of the spherical harmonic could be chosen for each iteration of processing. The coefficients were determined through a least-squares regression method and therefore the adequacy and accuracy can be examined through calculation of the coefficient of determination. The coefficient of determination was calculated at a specified order through the 31 frequency spectrum. An example of the resulting coefficient of determination data for the orders selected for this thesis can be seen in Appendix A Fig. 45.

The author elected to process the data at orders 1, 3, 5, 7 and 10 to determine the order for this thesis. Since previous techniques utilizing spherical harmonics used ten (Mobley, 2012) and seventh (Krebs & Thomann, 2008) order fits, these must be included in the analysis. The remaining orders were chosen in an attempt to provide enough comparison data that would aid the decision of choosing the order for this thesis.

The following three figures facilitated the selection of the spherical harmonic order that would be employed to the remainder of the data exploration in this thesis by enabling the determination of a reference frequency. The coefficient of determination was calculated across the 31 frequency spectrum at the five orders identified as seen in Fig. 35. Figure 36 was created in order to interrupt the frequency spectrum at 300 Hz and allow better visualization of the activity at the lower frequencies. A final technique to view low frequency behavior was employed by discontinuing the frequency spectrum at 1000 Hz and plotting on a logarithmic scale which can be seen in Fig. 37.

**Coefficient of Determination versus Frequency**

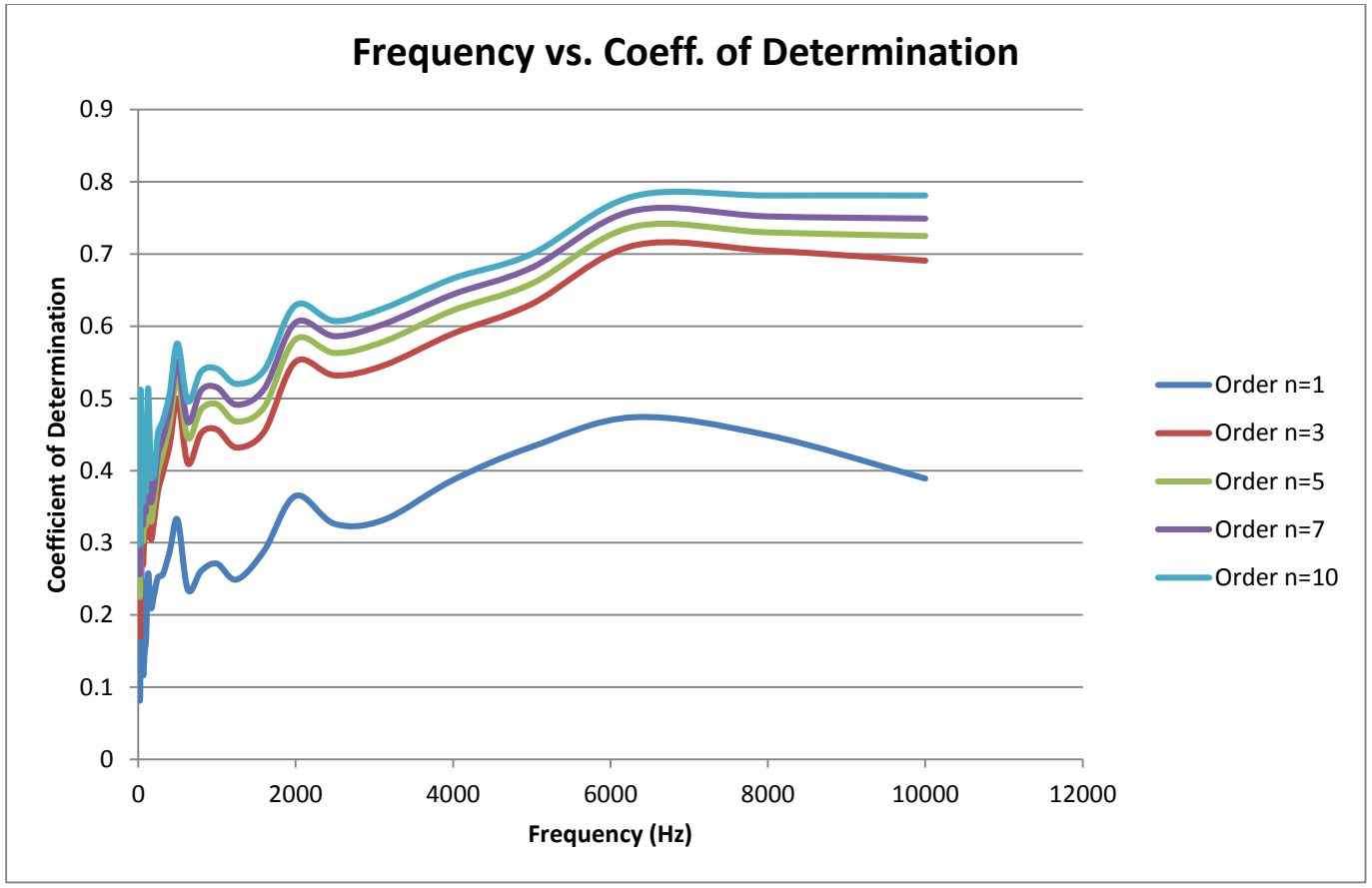


**Figure 35. Plot representing accepted 31 frequencies of the one-third octave band with the corresponding coefficient of determination at spherical harmonic orders one, three, five, seven and ten.**

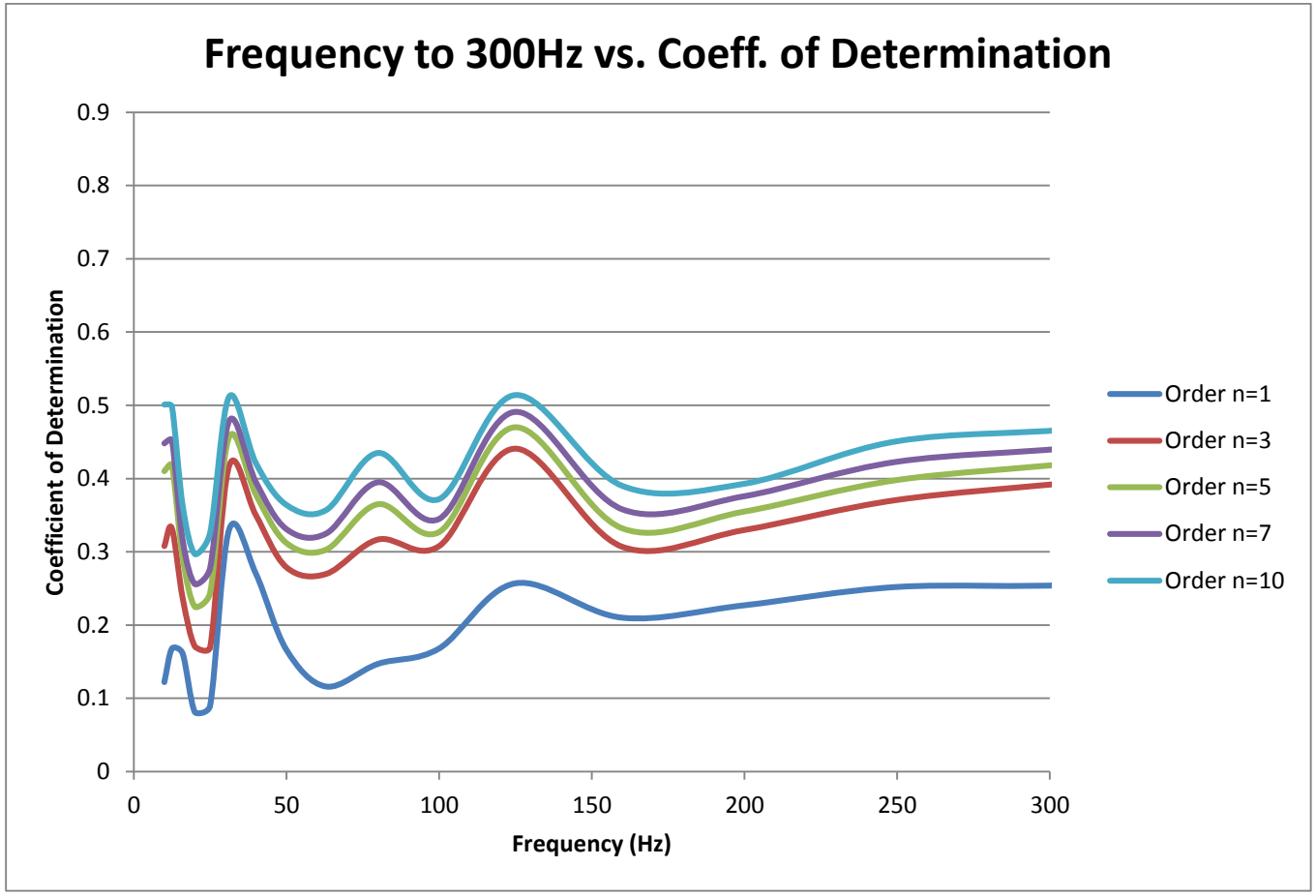


**Figure 36. Plot representing the accepted frequencies to 300 Hz of the one-third octave band with the corresponding coefficient of determination at spherical harmonic orders one, three, five, seven and ten.**

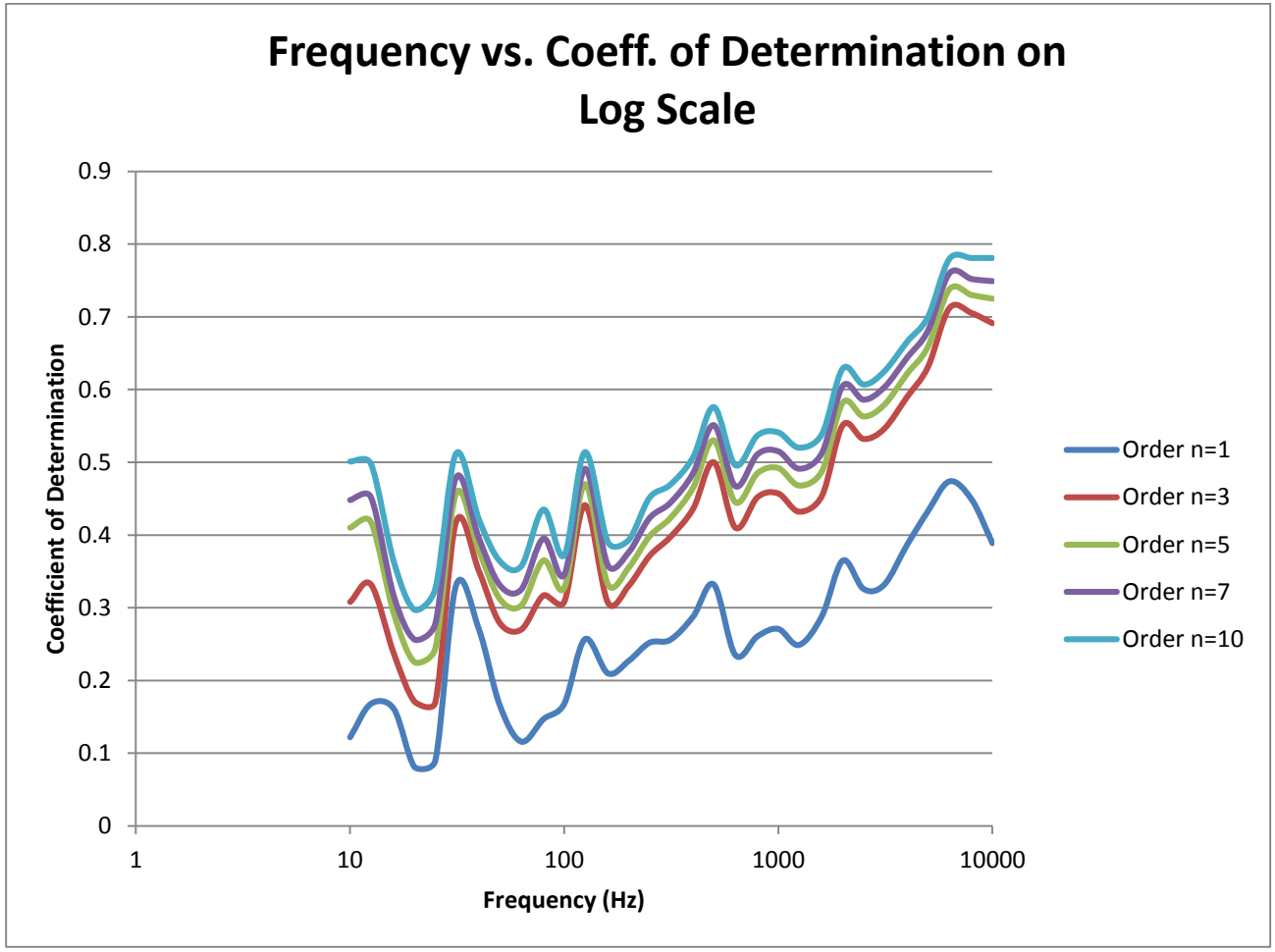


**Figure 37. Plot representing the accepted frequencies to 1000 Hz of the one-third octave band with the corresponding coefficient of determination at spherical harmonic orders one, three, five, seven and ten plotted on a logarithmic scale.**

### Coefficient of Determination versus Spherical Harmonic Order

In order to finalize the selection of the spherical harmonic order a reference frequency was selected utilizing the previous three figures. The coefficient of determination was next plotted against the five orders previously selected at the reference frequency of 125 Hz shown in Fig. 38.

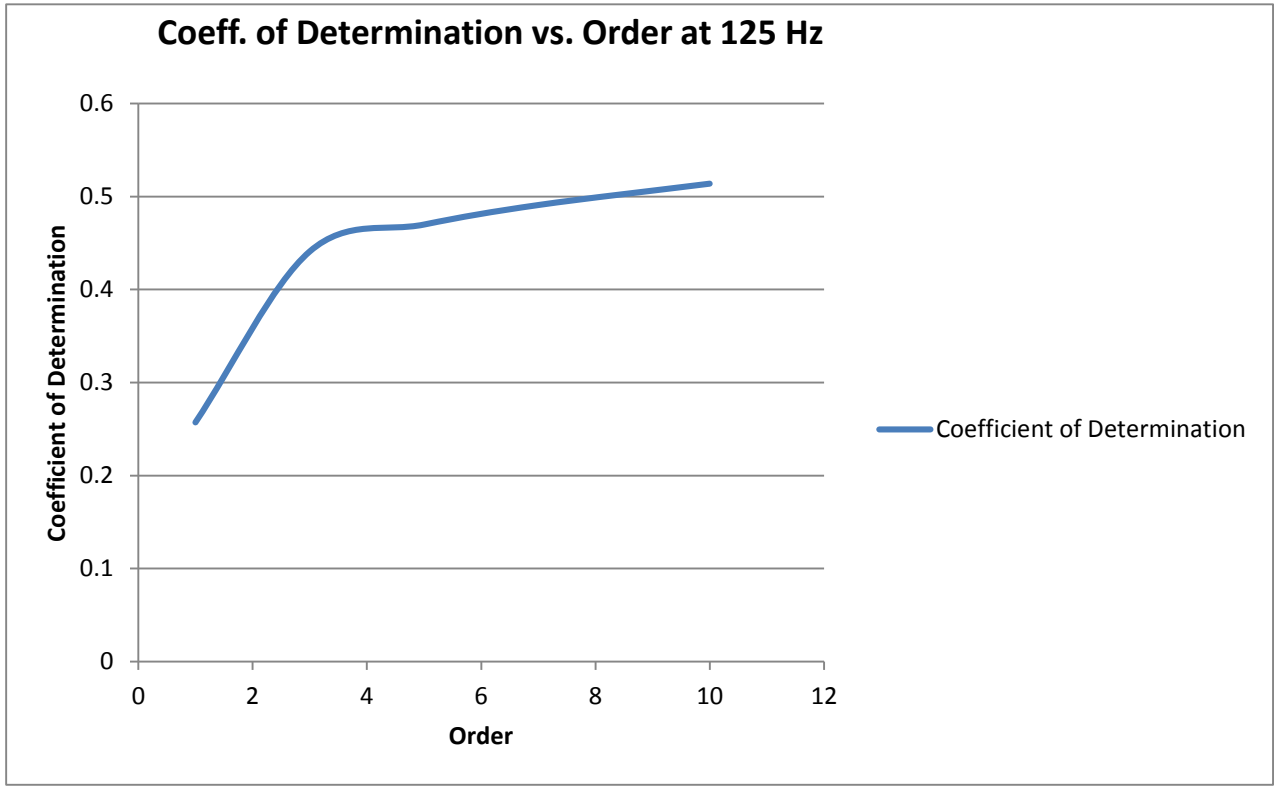


**Figure 38. Plot of the coefficient of determination at spherical harmonic orders one, three, five, seven and ten at 125 Hz reference frequency.**

A second reference frequency was selected for analysis purposes to assist with spherical harmonic order selection and the coefficient of determination was again plotted against the five orders previously selected. This is shown in Fig. 39 at the second reference frequency of 6300 Hz.

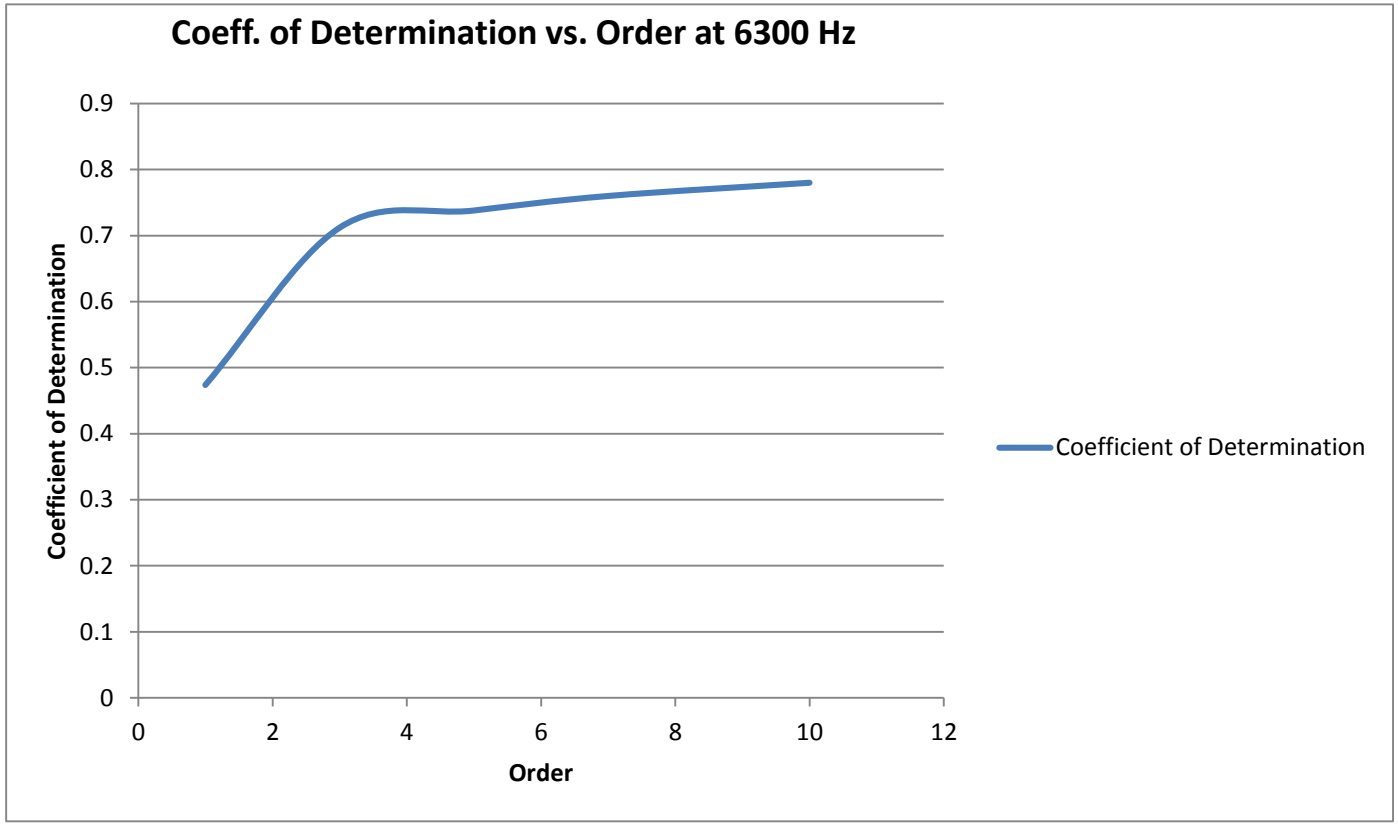


**Figure 39. Plot of the coefficient of determination at spherical harmonic orders one, three, five, seven and ten at the second reference frequency of 6300 Hz.**

## Validation

The LabVIEW programming code was also designed to compute the Sound Pressure Level (SPL) at each of the five chosen orders at each of the 31 frequencies and normalized to a one meter distance from the source center. These results are shown in appendix A Fig. 47. In order to compare the measured SPL with the measurement taken at the static validation microphone the measured data needed to be propagated to the distance the validation microphone was located at. In the data collection set up recall that the validation microphone was located two meters from the noise source. This propagation was completed by referencing Eqn. 15 where the losses propagated to two meters are subtracted from the predicted source level. Appendix A Fig. 46 displays the SPL data propagated at two meters for all five orders selected.

$$L_p = L_s + 20\log_{10}\left(\frac{1m}{2m}\right) = L_s - 6\ dB \tag{15}$$

The raw data collected at the static validation microphone was summed to a mean SPL at each of the 31 frequencies and a standard deviation was then computed for each frequency as well. Figure 40 shows the plot of the mean SPL data from the validation microphone, the standard deviation of the validation SPL data and the propagated SPL at two meters for each of the selected orders. In a similar manner as was conducted for the coefficient of determination plots, Fig. 41 displays the information on a logarithmic scale to aid in data analysis at the lower frequencies.

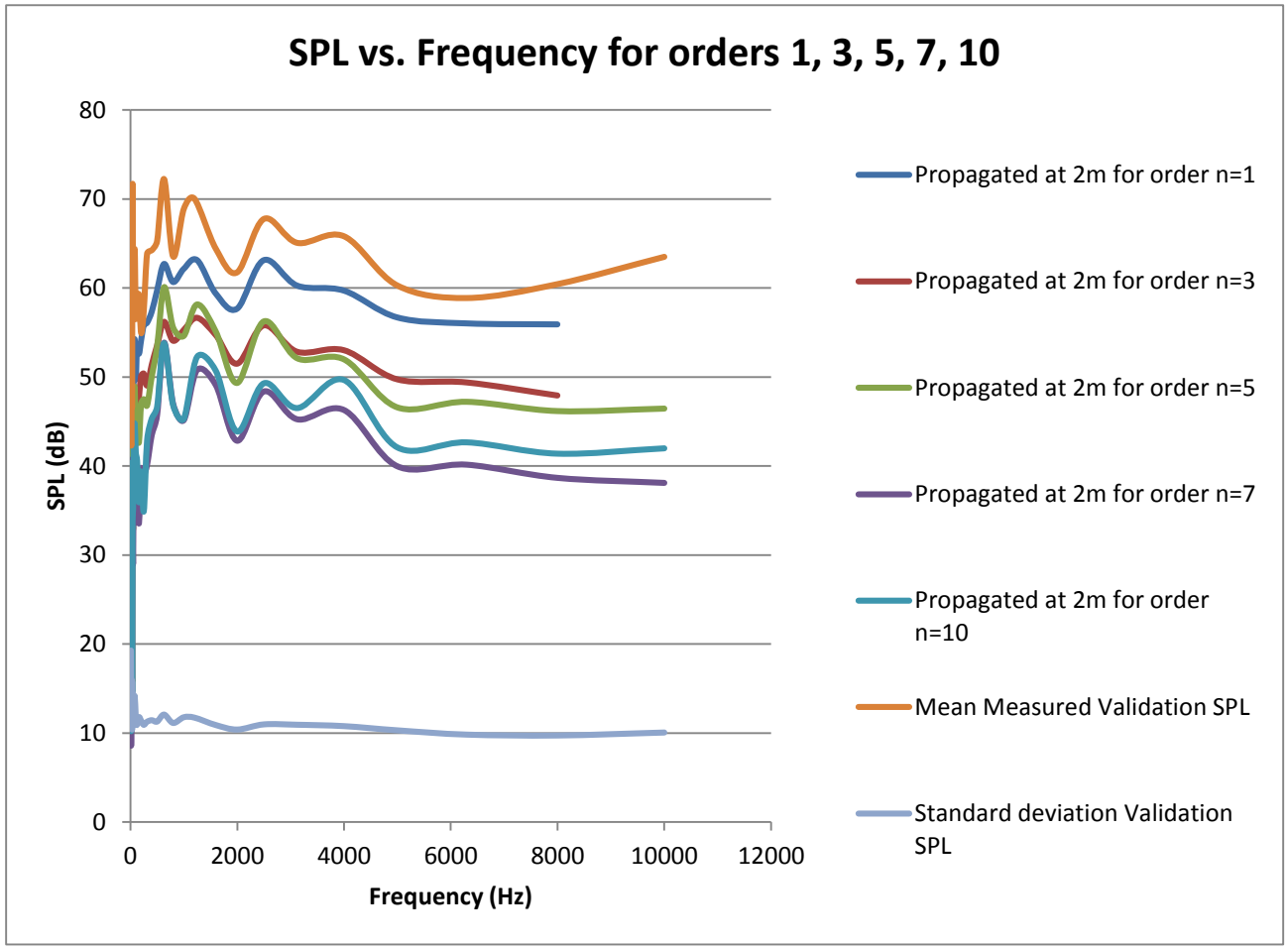


**Figure 40. Plot of the mean validation SPL data, the standard deviation of the validation SPL data and the propagated SPL at two meters for each of the selected spherical harmonic orders at the 31 frequencies.**

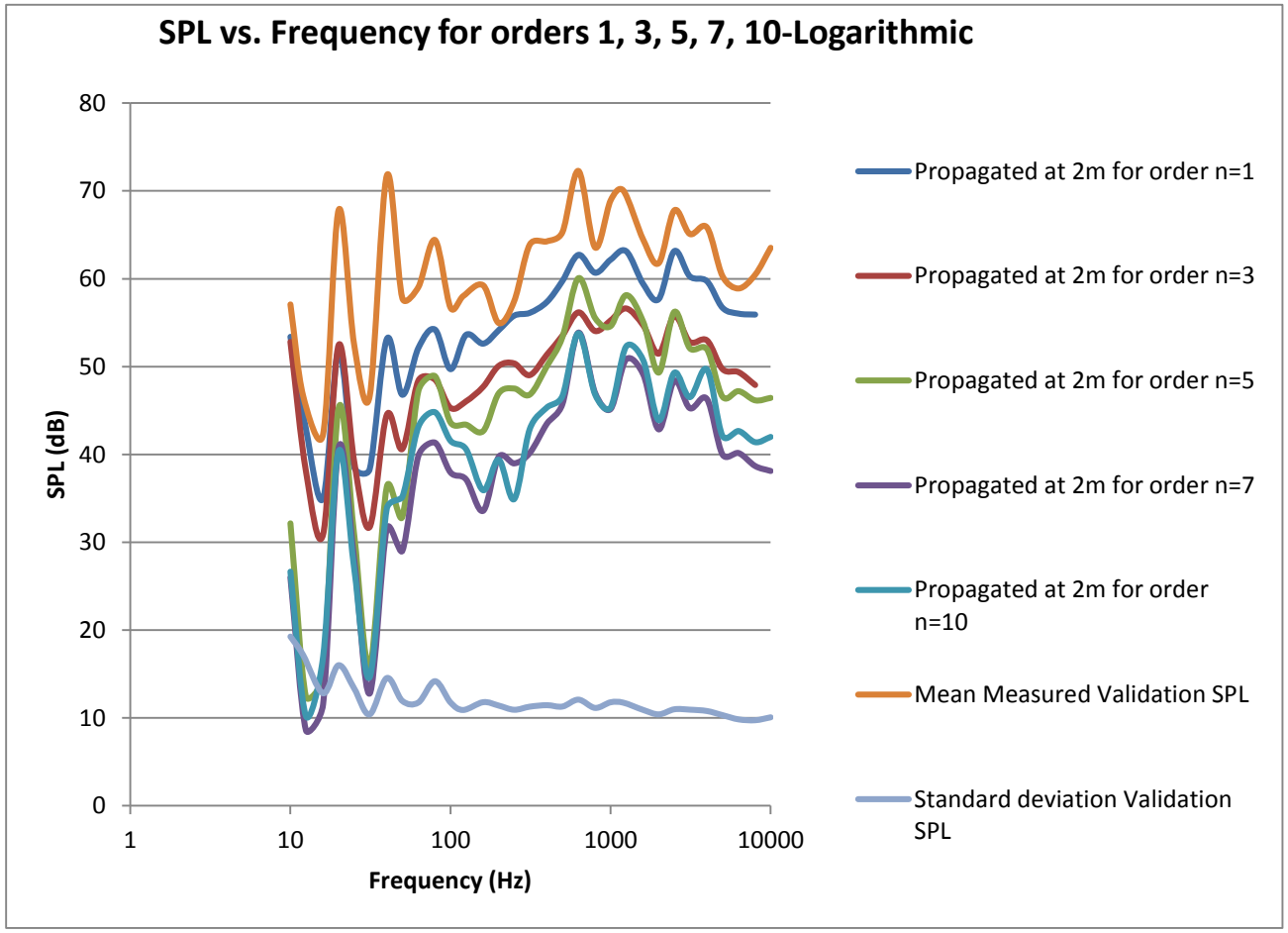


**Figure 41. Plot of the mean validation SPL data, the standard deviation of the validation SPL data and the propagated SPL at two meters for each of the selected spherical harmonic orders at the 31 frequencies on logarithmic scale.**

## V. Discussion

The previous sections of this thesis have explored some of the historical relevance of acoustic measuring and modeling. The author then outlined the process by which a data collection technique for a static noise source with a dynamic array was constructed and performed. The data captured by means of this technique has also been presented. This section will further explore and define the data presented and also assess the thesis methodology.

The data presented in the scatter plots was collected from the measurement of the compressor and presents both the measured and predicted source directivity patterns (see figures 33(a) and (b)). Visual analysis of both plots reveals agreement between the two. This validates the data collection technique for acquiring Sound Pressure Level (SPL) data and its accompanying location. The soundness of the measured and predicted source directivity pattern modeling method was also validated by the scatter plot agreement.

The waveform graph depicts the entire measured and predicted spectrum on the same plot. This visual comparison enables the ability to notice that although the measured data expressed in red (see figure 34) is oscillating and not in exact agreement with the predicted data expressed in white, there is good gross agreement. This suggests that the measurement methodology was reliable over the entire measurement spectrum.

Upon inspection of the coefficient of determination at each of the selected orders when viewed across all 31 frequencies, at low frequencies to 300 Hz and on a logarithmic scale (see figures 35-37) the author chose a reference frequency of 125 Hz. This frequency was selected

based on the majority of the orders being in close agreement at the low frequency and also having the highest coefficient of determination at the low frequencies.

After selecting the reference frequency of 125 Hz and plotting the coefficient of determination with respect to the five spherical harmonic orders previously chosen at this reference frequency as shown in Fig. 38, a spherical harmonic order was able to be decided. From analysis of this plot there is a leveling off of the coefficient of determination at or near order five. As the order increases, the accuracy of the coefficient of determination at 125 Hz approaches an asymptote of roughly 0.5. Thus, the author chose order five as the order to use for the spherical harmonic representation due to the fact that five was close enough to 0.5 without incurring the increased computation time for a small improvement in adequacy.

Recall the linear property of spherical harmonics and there is an expectation to observe the same or very similar shape in the plot of Fig. 38 at any other selected reference frequency within the frequency spectrum. To confirm this, the coefficient of determination at each of the selected orders viewed across all 31 frequencies in Fig. 35 are again examined. It is determined that there is a leveling off of the coefficient of determination around 6300 Hz frequency. Using this second reference frequency of 6300 Hz a plot of the coefficient of determination with respect to the five spherical harmonic orders previously chosen at this second reference frequency can be constructed (see figure 39). The same curve shape is observed at a 6300 Hz reference frequency as in Fig. 38 with a 125 Hz reference frequency. The leveling off of both curves remains near order five. The 6300 Hz reference frequency is better described due to the asymptotic behavior being at a higher coefficient of determination approaching 0.8.

The comparison of Figs. 38 and 39 detailing the coefficient of determination with respect to the five orders selected confirms the spherical harmonic order choice of five and validates the linear properties of the spherical harmonics. It is noted that increasing the order also increases the accuracy of the coefficient of determination regardless of the reference frequency. However, the increase in order does display asymptotic behavior that determines a discontinuation of increased accuracy at a certain order.

Once the spherical harmonic order was chosen to be five it was necessary to evaluate the SPL data at this specific order. Figure 42 shows the plot of the mean SPL data from the validation microphone, the standard deviation of the validation SPL data and the propagated SPL at two meters for order five across the 31 frequencies.

In similar fashion to the plots presented in the previous section, the SPL data displayed in Fig. 42 for order five only was also plotted to 100 Hz and on a logarithmic scale to aid in investigating (see figures 43-44). Upon inspection of the SPL plots for order five it can be determined that the propagated SPL at two meters is within ten decibels (dB) of the measurement taken at the static validation microphone.

Through analysis it is determined that if the order had been chosen to be seven there would have been approximately 10 dB loss from the order five results in comparison to the mean validation SPL. By exploring the next higher order, ten, it is determined that there is a slight advantage over order seven and a gain of approximately three to five dB. However, neither order seven nor order ten produced results that were closer than order five to the mean validation SPL.

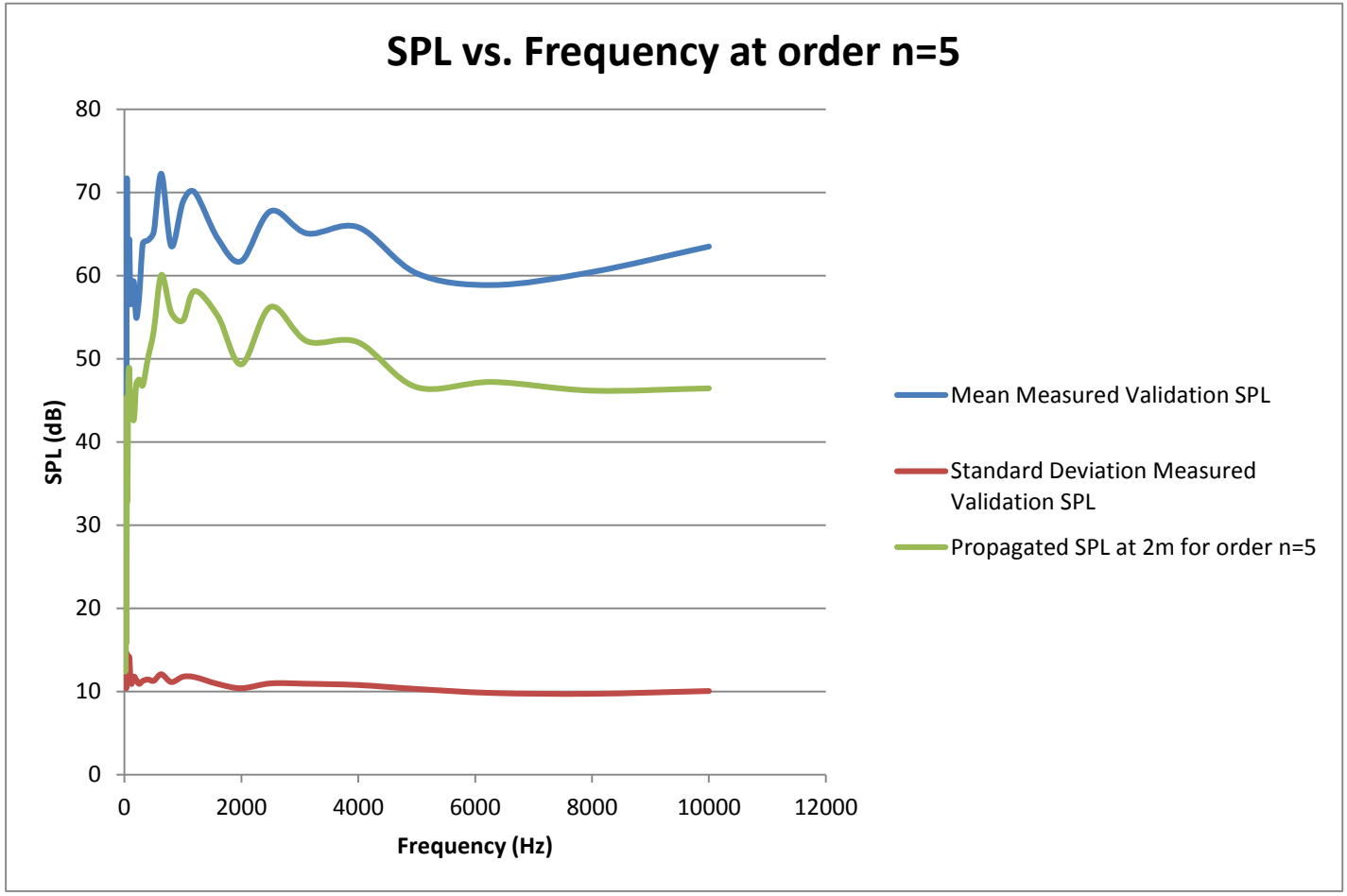


**Figure 42. Plot of the mean validation SPL data, the standard deviation of the validation SPL data and the propagated SPL at two meters for spherical harmonic order n=5 at the 31 frequencies.**

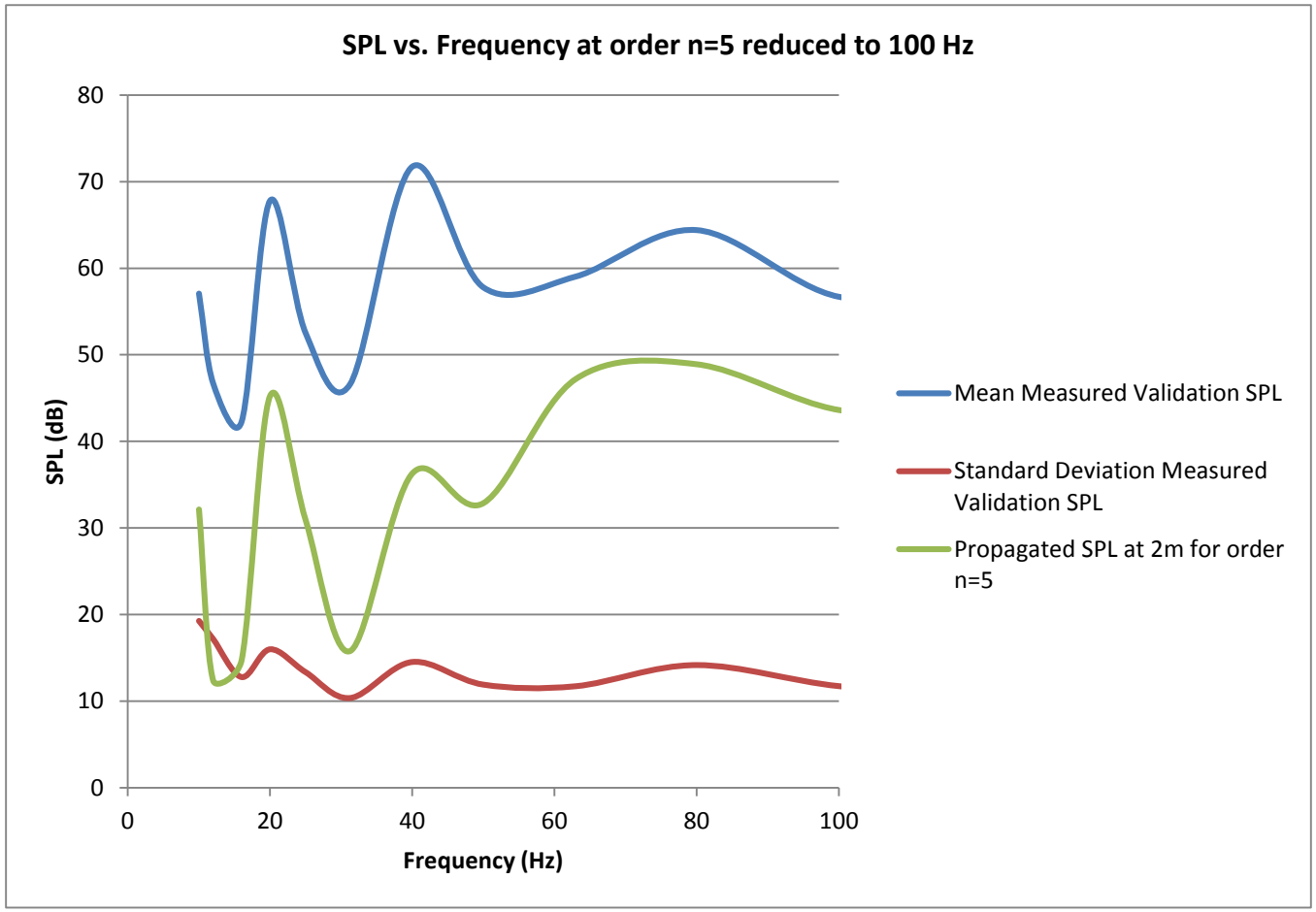


**Figure 43. Plot of the mean validation SPL data, the standard deviation of the validation SPL data and the propagated SPL at two meters for spherical harmonic order n=5 reduced to 100 Hz.**

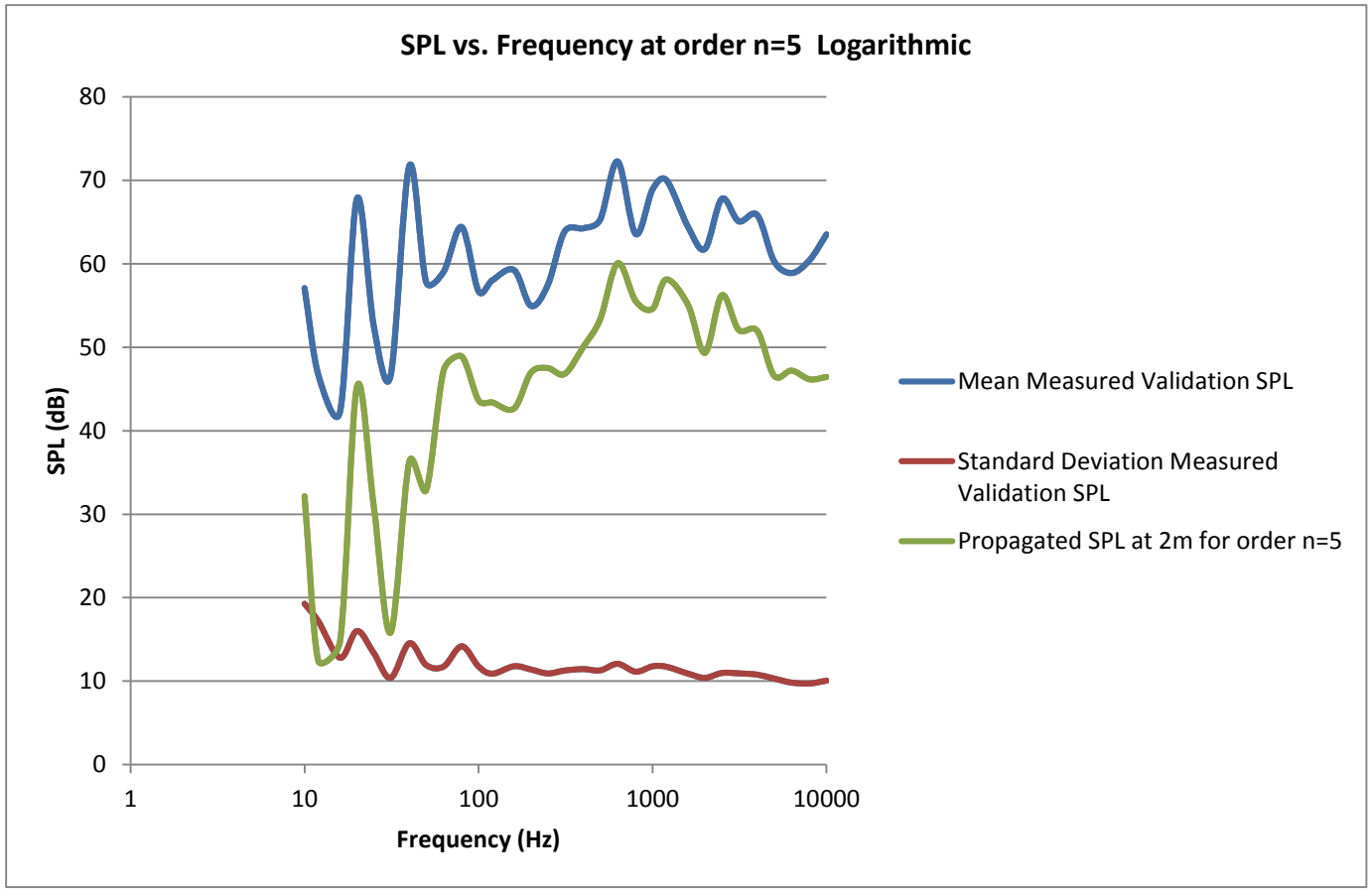


**Figure 44. . Plot of the mean validation SPL data, the standard deviation of the validation SPL data and the propagated SPL at two meters for each of the selected spherical harmonic orders at the 31 frequencies on logarithmic scale.**

## VI. Conclusions

This thesis intended to research and leverage historical methodologies concerning acoustic measurements with static arrays and both dynamic and static sources and the associated spherical harmonic modeling techniques. Software was programmed for the data acquisition of a man-portable dynamic microphone array location and acoustic Sound Pressure Level (SPL) at that location. A measurement conducted on a static air compressor with the dynamic array collected SPL and accompanying array location data. Simultaneously, acoustic SPL data was acquired at a fixed distance from the noise source by means of a second validation microphone. Both the dynamic array and static validation microphone data was processed, analyzed and modeled leveraging the techniques identified in the historical methodologies research and the conclusions are presented in the remainder of this section.

This thesis was determined to have satisfactory results based on the overall concept and process of utilizing a head-tracker sensor in combination with a microphone array to identify the SPL at specific locations. Also, identifying the electromagnetic interference of the metal mesh floor in the anechoic chamber and moving to a site that minimized the interference with the head-tracker source cube enabled suitable data results. Adequate results can also be identified through the use of leveraging the spherical harmonic methods researched for orders seven and ten to construct a hemisphere of an acoustic source. Further leveraging of this practice led to identify the spherical harmonic order of five that was then employed throughout the remainder of the thesis. Finally, the LabVIEW software that enabled the coordinate system to be centered on the source, collect the location and SPL data and process the data with spherical harmonics

leading to graphical representations proved to be acceptable. These plots revealed up to a twenty decibel difference, or two standard deviations from the measured and propagated data.

This difference can be accounted for from the near-field measurement along with the spatial limitation of the room to the nyquist relationship. The data collected at the near field does not describe what is occurring in the far-field because the data hasn't had a chance to establish in the far-field. Since frequency can be defined as the inverse of wavelength as well as the inverse of the period these can be equated, thus enabling a comparison over the same period. For example, taking 1000 samples at a 10 KHz frequency and then plotting the samples over a period would yield usable results. In contrast, collecting 1000 samples at a lower frequency of 10 Hz over the same period would not yield useable results.

Recall that the room was limited to twelve feet by eight feet and the head-tracker sensor could only collect accurate position data five feet from the source cube. The two standard deviation results may be improved upon if the measurement could be taken further from the source at distances of 50 to 100 feet. Taking a measurement 100 feet from the source, in the far-field, should not express all the noise that is seen in the near-field measurements. Since the far-field wavelength is larger than the one-meter normalization used, a proper choice for spherical harmonic order could be zero. It is possible that the higher order terms could be fitted to the noise from the near-field collection.

There is also the path of exploring the polar directivity in a manner that could help in determining the proper spherical harmonic order. This method too could potentially assist in addressing the two standard deviation results. Based on addressing the limitations of the data

collection the author deemed twenty decibels a satisfactory difference to account for a successful procedure.

Based on the above conclusion that the methodology is sound, accuracy could have been improved if the head-tracker hardware was not insufficient to meet the needs of this thesis. The location data given by the head-tracker proved to be inaccurate at times. As can be seen in the scatter plots representing the measured and predicted data (see Fig. 33) the anomalous data is a direct result of the head-tracker not being able to accurately capture and represent the proper locations. Even after the anechoic chamber floor was identified as an error source and mitigated, the location of the metal source in between the head-tracker sensor and source cube during points of the measurement can account for error in the location data. Additionally, the placement of the head-tracker source cube in close proximity of a metal compressor provided inaccuracies in the location data. The opportunity for error also existed during measurement if the dynamic microphone was not consistently in the best position to collect the SPL magnitude accurately. It is necessary to ensure through the "tooth brush" or "arching" methods that the microphone is constantly positioned to maximize exposure to the source. Addressing the physical microphone orientation could potentially aid in improved data being collected. These limitations could potentially improve the accuracy of this methodology.

Consideration should be given to the object being measured in order to account for the potential electromagnetic interferences in future work within this thesis methodology. Other recommendations include consideration in selection of the type of head-tracker. If using the Polhemus or a similar source-sensor type head-tracker for data collection in an electromagnetic

environment the measurement could be aided by shielding the head-tracker source cube from the electromagnetic irritant. This thesis did not account for any reflections that were received by either the measurement or validation microphones. The two locations where the measurements were conducted in this thesis minimized reflections. However, a further exploration into the removal of any captured reflections could impact the accuracy of the results. While moving the array around the source during measurement it was identified that cable management is a crucial factor to be considered. Identifying a set up that secured the source cube permanently during measurement and addresses trailing cable drag would attend to issues the author had with accidental displacements of the source cube and cable complications during measurement. Finally, extending the use of the National Instruments channel driver by constructing a four microphone array could assist in addressing the orientation of the microphones to the source and potentially ensure a more accurate SPL collection.

This thesis detailed the measurement and modeling techniques along with the spherical harmonic methods for the characterization of the three-dimensional acoustic directivity pattern of a stationary noise source. An overall assessment of this thesis suggests that the methodology of measuring a static noise source with a dynamic man-portable array is sound and achieved the objective of this endeavor.

## Bibliography


Acoustic Holography with a concentric ridge and open spherical microphone araary2009*IEEE* 2173-2176

Acoustic Repropagation technique and practical source characterization for simulation noise model databases2010*NOISE-CON 2010*Baltimore, Maryland

2001*Acoustic Repropagation Technique Version 2 (ART2)*Wyle LaboratoriesArlingtonWyle Laboratories

2004*Acoustic Repropagation Technique version 3 (ART3)*Wyle LaboratoriesArlingtonWyle Laboratories

ArfkenWebber2001*Mathematical Methods for Physicists*

Brenter K. S., &. F. (1994). Helecopter Noise Prediction: The Current Status and Future Direction. *Journal of Sound and Vibration* , 79-96.

Conner, D. A. (2002). *A Tool for Low Procedures Design and Community Noise Impact Assessment: The Rotocraft Noise Model (RNM).* Heli, Japan.

Default airctaft source description and methods to assess source data2006*IMAGINE Project*

Eyges. (1972). *The Classical Electromagnetic Field.* Addison Wesley.

Flight Acoustic Testing and Data Acquisition For the RNM2006*American Helicopter Society 62nd Annual Forum*Phoenix

FURTHER DEVELOPMENT OF 3-D ROTARY-WING ACOUSTIC DIRECTIVITY USING A SPHERICAL HARMONIC REPRESENTATION2012Dayton

Griffiths. (1999). *Introduction to Electrodynamics.* Pearson.

Jackson. (1999). *Classical Electrodynamics.* Hamilton Printing.

KrebsButikoferPlussThomann2003Modeling of Three-Dimensional Sound Directivity Patterns of Helecopters*Acta Acustica United with Acustica* 273-279

2008*Lateral directivity of aircraft noise*Paris

MartarelliRevelTomasini2002Experimental sensitivity analysis for near-field acoustic holography*International Conference on noise and vibration engineering*1799-1807Leuven

Modeling of the three-dimensional sound directivity patterns of helicopters2003*Acta Acustica united with Acustica 89*2273-279

Moulton, C. L. (1992). *Air Firce Procedure for Predicting Noise Around Airbases: Noise Exposure Model (NOISEMAP) Technical Report.* El Sequndo: Wyle Research.

National Aeronautics and Space Administration1991*Aeroacoustics of Flight Vehicles: Theory and Practice*HamptonNASA

Near-field Acoustical Holography System For Detailed Jet Noise Source Characterization2011*Air Force Small Business Innovative Research*

Ollerhead, L. &. (1969). A Theoretical Study of Helecopter Rotor Noise. *Journal of Sound and Vibration* , 197-222.

PietrzkoHofmann1988Prediction of A-Weighted Aircraft Noise Based on Measured Directivity Patterns*Applied Acoustics* 29-44

Plotkin, K. (2001). The Role of Aircraft Noise Simulation Models. *The 2001 International Congress and Exhibition on Noise Control Engineering.* The Hauge.

Reguarlization for improving the deconvolution in real-time-near-field acoustic holography2011*Journal of the Acoustical Society of America* 3777-3787

2008*Rotorcraft Noise Model Technical Reference and User Manual (version 7.1)*WR09-04Wyle LaboratoriesArlington

Salomons, E. M. (2001). *Computational Atmospheric Acoustics.* Norwell: Kluwer Acedemic Publishers.

Spherical Acoustical Holography of Low-Frequency Noise Sources1996*Applied Acoustics* 85-95

Wangsness. (1986). *Electromagnetic Fields.* Wiley & Sons.

## Appendix A

| Coefficient of Determination | | | | | |
|---|---|---|---|---|---|
| **Frequency (Hz)** | **Order n=1** | **Order n=3** | **Order n=5** | **Order n=7** | **Order n=10** |
| 10 | 0.122 | 0.308 | 0.41 | 0.448 | 0.501 |
| 12.5 | 0.168 | 0.332 | 0.418 | 0.452 | 0.498 |
| 16 | 0.161 | 0.237 | 0.292 | 0.316 | 0.363 |
| 20 | 0.081 | 0.171 | 0.225 | 0.256 | 0.297 |
| 25 | 0.09 | 0.17 | 0.244 | 0.278 | 0.326 |
| 31.25 | 0.331 | 0.418 | 0.457 | 0.479 | 0.512 |
| 40 | 0.27 | 0.35 | 0.378 | 0.395 | 0.421 |
| 50 | 0.166 | 0.279 | 0.312 | 0.331 | 0.364 |
| 63 | 0.116 | 0.27 | 0.303 | 0.325 | 0.357 |
| 80 | 0.147 | 0.317 | 0.365 | 0.395 | 0.435 |
| 100 | 0.168 | 0.308 | 0.327 | 0.345 | 0.372 |
| 125 | 0.257 | 0.441 | 0.47 | 0.491 | 0.514 |
| 160 | 0.21 | 0.307 | 0.332 | 0.358 | 0.39 |
| 200 | 0.227 | 0.33 | 0.355 | 0.376 | 0.393 |
| 250 | 0.252 | 0.371 | 0.398 | 0.423 | 0.451 |
| 312.5 | 0.256 | 0.397 | 0.423 | 0.444 | 0.469 |
| 400 | 0.288 | 0.436 | 0.465 | 0.485 | 0.507 |
| 500 | 0.332 | 0.5 | 0.53 | 0.551 | 0.576 |
| 630 | 0.235 | 0.41 | 0.445 | 0.467 | 0.496 |
| 800 | 0.261 | 0.452 | 0.485 | 0.511 | 0.537 |
| 1000 | 0.271 | 0.457 | 0.492 | 0.515 | 0.541 |
| 1250 | 0.249 | 0.432 | 0.468 | 0.491 | 0.52 |
| 1600 | 0.289 | 0.454 | 0.488 | 0.513 | 0.539 |
| 2000 | 0.365 | 0.551 | 0.582 | 0.605 | 0.629 |
| 2500 | 0.326 | 0.532 | 0.563 | 0.586 | 0.607 |
| 3125 | 0.332 | 0.546 | 0.579 | 0.603 | 0.625 |
| 4000 | 0.387 | 0.59 | 0.622 | 0.644 | 0.666 |
| 5000 | 0.433 | 0.631 | 0.659 | 0.681 | 0.7 |
| 6300 | 0.474 | 0.712 | 0.738 | 0.76 | 0.78 |
| 8000 | 0.449 | 0.705 | 0.73 | 0.752 | 0.781 |
| 10000 | 0.389 | 0.691 | 0.725 | 0.749 | 0.781 |

**Figure 45. Coefficients of determination for the five orders selected at each of the accepted 31 frequencies.**

| Propagated SPL at 2m | | | | | |
|---|---|---|---|---|---|
| **Frequency (Hz)** | **Order n=1** | **Order n=3** | **Order n=5** | **Order n=7** | **Order n=10** |
| 10 | 53.393 | 52.83 | 32.158 | 25.978 | 26.652 |
| 12.5 | 42.919 | 38.085 | 12.383 | 8.569 | 10.201 |
| 16 | 35.016 | 30.897 | 14.763 | 11.542 | 16.958 |
| 20 | 51.83 | 52.461 | 45.271 | 40.732 | 40.365 |
| 25 | 38.579 | 39.246 | 30.925 | 28.139 | 27.067 |
| 31.25 | 38.321 | 31.73 | 15.808 | 12.761 | 14.62 |
| 40 | 53.138 | 44.517 | 36.311 | 31.531 | 33.838 |
| 50 | 46.794 | 40.632 | 32.888 | 29.012 | 35.164 |
| 63 | 52.126 | 48.415 | 47.233 | 39.821 | 43.144 |
| 80 | 54.217 | 48.534 | 48.925 | 41.334 | 44.813 |
| 100 | 49.71 | 45.309 | 43.642 | 37.943 | 41.558 |
| 125 | 53.612 | 46.054 | 43.397 | 37.157 | 40.608 |
| 160 | 52.616 | 47.714 | 42.669 | 33.572 | 35.923 |
| 200 | 54.144 | 50.089 | 46.958 | 39.712 | 39.407 |
| 250 | 55.797 | 50.374 | 47.511 | 38.971 | 34.919 |
| 312.5 | 56.117 | 49.04 | 46.816 | 40.154 | 42.889 |
| 400 | 57.361 | 51.373 | 50.066 | 43.49 | 45.348 |
| 500 | 59.741 | 53.536 | 53.373 | 45.721 | 46.657 |
| 630 | 62.719 | 56.193 | 60.087 | 53.863 | 53.811 |
| 800 | 60.679 | 54.063 | 55.549 | 46.996 | 46.838 |
| 1000 | 62.167 | 55.273 | 54.619 | 45.156 | 45.327 |
| 1250 | 63.14 | 56.64 | 58.147 | 50.81 | 52.294 |
| 1600 | 59.381 | 54.698 | 55.085 | 49.079 | 50.703 |
| 2000 | 57.69 | 51.49 | 49.33 | 42.839 | 43.889 |
| 2500 | 63.143 | 55.79 | 56.247 | 48.377 | 49.312 |
| 3125 | 60.274 | 52.823 | 52.099 | 45.251 | 46.526 |
| 4000 | 59.716 | 53 | 51.978 | 46.294 | 49.68 |
| 5000 | 56.701 | 49.728 | 46.583 | 39.97 | 42.102 |
| 6300 | 56.031 | 49.381 | 47.213 | 40.153 | 42.671 |
| 8000 | 55.92 | 47.914 | 46.168 | 38.668 | 41.4 |
| 10000 | 56.601 | 47.239 | 46.448 | 38.104 | 42 |

**Figure 46. Propagated SPL at two meters for the five orders selected at each of the accepted 31 frequencies**

| Propagated SPL at 1m | | | | | |
|---|---|---|---|---|---|
| **Frequency (Hz)** | **Order n=1** | **Order n=3** | **Order n=5** | **Order n=7** | **Order n=10** |
| 10 | 59.393 | 58.83 | 38.158 | 31.978 | 32.652 |
| 12.5 | 48.919 | 44.085 | 18.383 | 14.569 | 16.201 |
| 16 | 41.016 | 36.897 | 20.763 | 17.542 | 22.958 |
| 20 | 57.83 | 58.461 | 51.271 | 46.732 | 46.365 |
| 25 | 44.579 | 45.246 | 36.925 | 34.139 | 33.067 |
| 31.25 | 44.321 | 37.73 | 21.808 | 18.761 | 20.62 |
| 40 | 59.138 | 50.517 | 42.311 | 37.531 | 39.838 |
| 50 | 52.794 | 46.632 | 38.888 | 35.012 | 41.164 |
| 63 | 58.126 | 54.415 | 53.233 | 45.821 | 49.144 |
| 80 | 60.217 | 54.534 | 54.925 | 47.334 | 50.813 |
| 100 | 55.71 | 51.309 | 49.642 | 43.943 | 47.558 |
| 125 | 59.612 | 52.054 | 49.397 | 43.157 | 46.608 |
| 160 | 58.616 | 53.714 | 48.669 | 39.572 | 41.923 |
| 200 | 60.144 | 56.089 | 52.958 | 45.712 | 45.407 |
| 250 | 61.797 | 56.374 | 53.511 | 44.971 | 40.919 |
| 312.5 | 62.117 | 55.04 | 52.816 | 46.154 | 48.889 |
| 400 | 63.361 | 57.373 | 56.066 | 49.49 | 51.348 |
| 500 | 65.741 | 59.536 | 59.373 | 51.721 | 52.657 |
| 630 | 68.719 | 62.193 | 66.087 | 59.863 | 59.811 |
| 800 | 66.679 | 60.063 | 61.549 | 52.996 | 52.838 |
| 1000 | 68.167 | 61.273 | 60.619 | 51.156 | 51.327 |
| 1250 | 69.14 | 62.64 | 64.147 | 56.81 | 58.294 |
| 1600 | 65.381 | 60.698 | 61.085 | 55.079 | 56.703 |
| 2000 | 63.69 | 57.49 | 55.33 | 48.839 | 49.889 |
| 2500 | 69.143 | 61.79 | 62.247 | 54.377 | 55.312 |
| 3125 | 66.274 | 58.823 | 58.099 | 51.251 | 52.526 |
| 4000 | 65.716 | 59 | 57.978 | 52.294 | 55.68 |
| 5000 | 62.701 | 55.728 | 52.583 | 45.97 | 48.102 |
| 6300 | 62.031 | 55.381 | 53.213 | 46.153 | 48.671 |
| 8000 | 61.92 | 53.914 | 52.168 | 44.668 | 47.4 |
| 10000 | 62.601 | 53.239 | 52.448 | 44.104 | 48 |

**Figure 47. Propagated SPL normalized at one meter for the five orders selected at each of the accepted 31 frequencies.**